# CancerPAM: A Multi-Omics Pipeline for Personalized CRISPR Knock-In Cytokine Gene Therapy to Remodel the Tumor Microenvironment and Enhance CAR T Cell Therapy in Solid Tumors

# - Supplement -

## Content

List of Abbreviations	3
Supplementary Notes	4
Supplementary Note 1	4
Supplementary Note 2	4
Supplementary Note 3	4
Supplementary Note 4	4
Supplementary Note 5	4
Supplementary Note 6	4
Supplementary Note 7	5
Supplementary Note 8	5
Supplementary Note 9	5
Supplementary Note 10	5
Supplementary Note 11	5
Supplementary Note 12	5
Supplementary Note 13	5
Supplementary Note 14	6
Supplementary Methods	7
Genomic DNA Sample Isolation	7
Standard PCR	7
Evaluation of Cell Proliferation and Viability Following CRISPR/Cas9-Mediated Gene Integration	7
Cytokine Quantification via ELISA	7
Flow Cytometry and Fluorescence-Activated Cell Sorting (FACS)	7
Boyden chamber and Clearview trans well migration assays	8
Generation of L1CAM knock-out SK-N-BE2c	8
Immunohistochemistry (IHC)	8
Supplementary Figures	10
Supplementary Fig. S1. CancerPAM multiomics-based automated pipeline.	10
Supplementary Fig. S2. Dataset comparison between Terminate NB and DepMap	11
Supplementary Fig. S3. Cell line data comparison between Terminate NB and DepMap data sets	12
Supplementary Fig. S4. Chromosomal novel PAM distribution	13
Supplementary Fig. S5. Novel PAM feature characteristics distribution.	14
Supplementary Fig. S6. CancerPAM ranking validation.	15
Supplementary Fig. S7. Feature correlation with PAM count.	16
Supplementary Fig. S8. Influence of MYCN amplification status on novel PAM counts and features	17
Supplementary Fig. S9. In vitro CRISPR cutting and transgene vector production and testing	18

	Supplementary Fig. S10. In vitro CRISPR knock-in.	19
	Supplementary Fig. S11. Site-specific knock-in confirmation via Sanger sequencing and PAM frequency analysis.	20
	Supplementary Fig. S12. Site-specific knock-in analysis via dPCR and IFNG toxicity testing.	21
	Supplementary Fig. S13. Unspecific T cell knock-in	22
	Supplementary Fig. S14. dPCR analysis after FACS enrichment.	23
	Supplementary Fig. S15. Characterization of enriched transgenic tumor cell lines.	24
	Supplementary Fig. S16. CAR T cell activation and exhaustion in tumor cell line—CAR T cell co-culture experiment	
	Supplementary Fig. S17. Cytokine secretion in tumor cell line—CAR T cell co-culture experiments	26
	Supplementary Fig. S18. Cytokine-mediated T cell migration in vitro	27
	Supplementary Fig. S19. 3D tumor infiltration assay.	28
	Supplementary Fig. S20. In vivo CAR T cell infiltration model development	29
	Supplementary Fig. S21. In vivo CAR T cell infiltration experiment: pre-transplant and pre-treatment analysis	30
	Supplementary Fig. S22. Bioluminescence imaging of CAR T cell treated SK-N-AS xenograft neuroblasoma model	ls.31
	Supplementary Fig. S23. Bioluminescence imaging of CAR T cell treated SK-N-BE2c xenograft neuroblasoma mod	
	Supplementary Fig. S24. In vivo CAR T cell infiltration in CXCL10-secreting xenograft tumors	33
	Supplementary Fig. S25. Immunofluorescence staining of tumor sections.	34
S	upplementary Tables	35
	Supplementary Table 1. Exemplary patient data for top and bottom rank novel PAM sites identified via CancerPA	
	Supplementary Table 2. Neuroblastoma cell line target loci	35
	Supplementary Table 3. HDRT sequences	36
	Supplementary Table 4. Primer and probe sequences	37
	Supplementary Table 5. Equipment and Consumables used	38
	Supplementary Table 6. Antibodies used for flow cytometry and IF Staining	42
	Supplementary Table 7. Software used	43

## List of Abbreviations

AAV - Adeno-associated virus

AUC – Area under the curve

BLI - Bioluminescence Imaging

CAR - Chimeric antigen receptor

CFD – Cutting frequency determination

cDNA – Complementary DNA

CI - Confidence Interval

CMV – Cytomegalovirus (used as a promoter in gene expression)

CRISPR - Clustered regularly interspaced short palindromic repeats

DepMap – Cancer Dependency Map

dPCR – Digital polymerase chain reaction

 $ds DNA-Double\text{-}stranded\ DNA$ 

EF1a – Elongation factor 1 alpha (used as a promoter in gene expression)

ELISA – Enzyme-linked immunosorbent assay

EGFRt – Truncated epidermal growth factor receptor

FACS - Fluorescence-activated cell sorting

FBS – Fetal bovine serum

FMO - Fluorescence minus one

GFP – Green fluorescent protein

gRNA - Guide RNA

HDR - Homology-directed repair

HDRT – Homology-directed repair template

HUVEC - Human Umbilical Vein Endothelial Cells (used in the trans-

endothelial migration assay) IFNG – Interferon-gamma

IL-2 – Interleukin-2

IL-7 – Interleukin-7

IL-15 – Interleukin-15

L1CAM - L1 cell adhesion molecule

LNP - Lipid nanoparticle

LTR - Long terminal repeat

MACS – Magnetic-activated cell sorting

 $\mathsf{MFI}-\mathsf{Mean}\ \mathsf{fluorescence}\ \mathsf{intensity}$ 

MIT – Massachusetts Institute of Technology (used in CRISPR

specificity scoring)

NGG – Most common protospacer adjacent motif (PAM)

recognized by SpCas9

NK – Natural killer (cells)

NSG - NOD-scid IL2Rynull (immunodeficient mouse model)

PAM – Protospacer adjacent motif PBS – Phosphate-buffered saline

PBMCs – Peripheral blood mononuclear cells

PCR - Polymerase chain reaction

PE - Phycoerythrin

Pen/Strep - Penicillin/Streptomycin

qPCR - Quantitative polymerase chain reaction

Q8 – Custom reporter epitope tag (CD34 epitope and CD8

transmembrane domain)

REP - Rapid expansion protocol

RNP - Ribonucleoprotein

RPMI – Roswell Park Memorial Institute (medium)

SD - Standard deviation

sgRNA – Single-guide RNA

SNV – Single nucleotide variant

SORT – Selective organ targeting

sPA – Synthetic poly(A) sequence

TAE – Tris-acetate-EDTA (buffer for electrophoresis)

TME – Tumor microenvironment

TRAC - T cell receptor alpha constant

UV – Ultraviolet

VEGF – Vascular Endothelial Growth Factor

WES - Whole-exome sequencing

WGS – Whole-genome sequencing

## **Supplementary Notes**

## Supplementary Note 1

The increased frequency of novel PAM sites in neuroblastoma cell lines was associated with a higher prevalence of mutations toward cytosine (C) or guanine (G), as observed in these datasets (Supplementary Fig. S2c).

## Supplementary Note 2

The FCGBP gene harbored five or more novel PAMs across all terminate NB cell lines, yet it did not exhibit a similar prominence in patient samples. Notably, there was no overlap between the top 10 genes with the highest novel PAM counts in cell lines and those in patient-derived data (Fig. S1E). In patient exome data, DLG2 (Chr. 11) emerged as the gene with the highest prevalence of at least one novel PAM site, identified in 13 out of 54 patients (Supplementary Fig. S1f). Across all patient samples, 17 novel PAM sites were recurrently identified in two individuals.

#### Supplementary Note 3

To further investigate discrepancies between cell lines and patient data, we applied CancerPAM to publicly available whole-exome sequencing (WES) datasets from 48 neuroblastoma cell lines (including eight from our dataset) available on the DepMap portal. In DepMap 23Q4, a median of 25 novel PAMs were identified from 155 SNVs (19% [95% CI: 17–22%]), a value more consistent with patient-derived data compared to terminate NB cell line data (Supplementary Fig. S2a). However, cross-comparison of different DepMap versions (20Q4, 22Q2 and 23Q4) for the same 48 cell lines revealed inconsistencies. DepMap 23Q4 reported fewer SNVs and novel PAMs, with only partial overlap between versions (Supplementary Fig. S2b,c). Additionally, DepMap 23Q4 exhibited a significantly lower percentage of SNVs relative to the terminate NB dataset (Supplementary Fig. S2d). Surprisingly, the concordance of SNVs between DepMap datasets and terminate NB was low, with only 46% of SNVs from DepMap 23Q4 and 45% from DepMap 20Q4/22Q2 overlapping with terminate NB, despite terminate NB reporting nearly 10-fold more SNVs than DepMap 23Q4 (median 1,470 vs. 155 SNVs) (Supplementary Fig. S2e,g, S3). As expected, a gene-level analysis of chromosomes 1 and 19 revealed a higher proportion of genes with at least two novel PAM sites in terminate NB, reinforcing the increased mutation burden in these datasets. Only three genes on Chr. 1 and none on Chr. 19 harbored at least two novel PAMs shared across both datasets (Supplementary Fig. S4).

## Supplementary Note 4

When analyzing the correlation of other features besides CRISPR specificity scores with the total PAM count per patient, a similar, albeit weaker, effect was observed for CRISPR efficiency scores, while no significant correlation was detected for copy number or gene expression. However, the copy number of top-ranked PAM sites was positively correlated with the total number of PAMs detected per patient, suggesting a potential structural genomic influence on PAM site availability (Supplementary Fig. S7).

## Supplementary Note 5

To explore possible confounding factors, we examined the correlation between PAM feature characteristics and MYCN amplification status. Analysis of DepMap 23Q4 data indicated a slightly higher proportion of novel PAM sites located in non-essential genes in MYCN non-amplified cell lines. However, the observed effect size was marginal (median difference of 1.1%), and the findings could not be reproduced in the eight terminate NB cell lines with available dependency data, indicating that MYCN amplification status is unlikely to be a major determinant of PAM site distribution (Supplementary Fig. S8).

## Supplementary Note 6

Preliminary CRISPR cutting efficiency experiments demonstrated relevant cutting activity (>5%) at all loci, except for *SCAF11*, *SH3BP1* and *SNX18*. The measured relative cutting frequency exhibited only a weak positive correlation with the Doench score and showed no correlation with the Moreno score. However, the strongest correlation - albeit not statistically significant - was observed for higher copy number regions (Supplementary Fig. S9a, b).

## Supplementary Note 7

Optimization of HDRT constructs for knock-in revealed that a custom-designed EF1a-derived shortened promoter in combination with a Q8 (CD8 transmembrane + CD34 Qbend epitope) reporter exhibited the highest knock-in efficiency. In contrast, HDRTs incorporating a larger hCMV promoter or fluorophores such as RFP and GFP showed reduced efficiency, likely due to their increased genetic payload. We also tested a multicistronic vector encoding two cytokines, which demonstrated stable knock-in at the AAVS1 locus but with significantly lower efficiency.

## Supplementary Note 8

We also evaluated a combinatorial knock-in strategy using two HDRTs (differing homology arms) and two gRNAs (targeting distinct tumor-specific loci) simultaneously, without increasing total DNA or gRNA dosage. This approach led to increased reporter expression after 28 days (Supplementary Fig. S10b). However, despite its efficacy, this strategy was not pursued in subsequent experiments due to the potential risk of chromosomal translocation. Lastly, we observed significantly lower knock-in rates for IFNG, particularly in SK-N-BE2c, suggesting locus- or transgene-specific effects on knock-in efficiency (Fig. 3d, Supplementary Fig. S10c).

## Supplementary Note 9

Additional Sanger sequencing of Out/In PCR products provided definitive proof of on-target knock-ins (Supplementary Fig. S11a). Further analysis using Out/Out preferential amplification followed by Sanger sequencing and PAM site frequency determination confirmed the loss of the novel PAM site post-knock-in on a quantitative level (Supplementary Fig. S11c). Analysis of weak-positive dPCR signals indicated reduced performance and sensitivity of the Out/In dPCR assay used for investigating AAVS1 knock-ins, which explains the discrepancy between higher knock-in rates observed in flow cytometry compared to dPCR for AAVS1 knock-ins (Supplementary Fig. S12c).

## Supplementary Note 10

Unspecific knock-in, was assumedly not entirely due to CRISPR/Cas9-related effects, as transfection of high doses of Q8-HDRT alone also led to an increase in Q8+ positivity after 21 days - although this was not statistically significant- when compared to Q8+ positivity of control cells transfected with a GFP-HDRT. After subtracting the mean Q8+ count, only *IGSF9B* and *RPLPO* remained as gRNAs significantly associated with CRISPR-mediated unspecific knock-in (Fig. 4e, Supplementary Fig. S13c). The observed trend for inverse correlation between unspecific knock-in rates and CancerPAM ranking scores (Fig.4g,h) persisted after subtracting mean DNA-only transfection Q8+ cell counts (Supplementary Fig. S13d).

#### Supplementary Note 11

We did not observe any growth advantage or disadvantage in the enriched transgenic tumor cell lines, regardless of cell line, target locus, or cytokine combination (Fig. 5C, Supplementary Fig. S14a,b).

## Supplementary Note 12

During in vitro CAR T cell SK-N-AS tumor co-culture, we did not observe any differences in the expression of activation markers (CD25, CD137) or exhaustion markers (LAG3, TIM3, PD1), as measured via flow cytometry, among the different cytokine-expressing tumor cell lines (Supplementary Fig. S16b,c). Interestingly, co-culture with tumor cells resulted in elevated CXCL10 and CXCL11 levels in all CAR T cell plus unmodified or transgenic tumors, except when co-cultured with IFNG-expressing tumors. Regarding IFNG release, we observed that CAR T cell-mediated IFNG secretion was only a fraction of the levels produced by IFNG-transgenic tumors. CAR T cell IL-2 secretion remained unaffected by additional cytokine secretion from tumor cells (Supplementary Fig. S17).

## Supplementary Note 13

After confirming similar engraftment across all treatment groups, comparison of day 1 BLI data post-CAR T cell injection in the lung showed no significant differences between tumor groups (Supplementary Figs. S24a,b).

## Supplementary Note 14

Serum cytokine level analysis via ELISA confirmed CXCL10 expression in mice harboring transgene-positive tumors, both pre- and post-treatment (Supplementary Fig. S21a, S24f). Additionally, post-mortem immunofluorescence analysis of tumor sections confirmed persistent L1CAM positivity and low-abundance CD3+ T cells within tumors (Supplementary Fig. S25).

## Supplementary Methods

#### Genomic DNA Sample Isolation

Genomic DNA was extracted from cultured cells using the QIAamp DNA Mini Kit (QIAGEN) following the manufacturer's guidelines with minor optimizations. Briefly, up to  $5 \times 10^6$  cells were lysed using Proteinase K and buffer AL at  $56^{\circ}$ C, followed by ethanol precipitation. The lysate was passed through a QIAamp Mini Spin Column via centrifugation to bind DNA, followed by sequential washes with AW1 and AW2 buffers to remove contaminants. Purified DNA was eluted in Buffer AE and stored at -20°C until further use.DNA concentration and purity were assessed using a NanoDrop 2000 spectrophotometer (Thermo Fisher Scientific) at 260 nm absorbance, ensuring concentrations  $\geq 10$  ng/ $\mu$ L for downstream applications.

#### Standard PCR

PCR was performed using KAPA polymerase (Roche) to amplify DNA sequences for homology-directed repair templates (HDRTs), target sequencing and qualitative knock-in analysis. Primers were custom-designed using SnapGene (GSL Biotech LLC) and Primer3Plus (https://www.primer3plus.com/) and Primer-BLAST (NCBI). PCR reactions were carried out using a C1000 Touch Thermal Cycler (Bio-Rad) under optimized cycling conditions. For sequence analysis, amplified fragments purified using the QIAquick PCR Purification Kit (QIAGEN) and sequenced by LGC Genomics. PCR product specificity and efficiency were confirmed by agarose (1-2%) gel-electrophoresis using TAE buffer-based gels, with GelRed (Sigma-Aldrich) staining for visualization. A detailed list of primers and oligonucleotides used in the study is provided in **Supplementary Table 4**.

## Evaluation of Cell Proliferation and Viability Following CRISPR/Cas9-Mediated Gene Integration

Genome-edited SK-N-BE2c and SK-N-AS neuroblastoma cell lines, along with their wild-type counterparts, were used for proliferation and viability assessments. Cell proliferation was monitored over seven days using the IncuCyte® Live-Cell Analysis System (Sartorius). Cells were seeded in 96-well flat-bottom plates at  $1 \times 10^4$  cells per well in biological duplicates and technical triplicates. Phase-contrast imaging was performed at regular intervals to generate quantitative growth curves. Viability was assessed using IncuCyte® Cytotox Green reagent (Sartorius, catalog #4633) at a final concentration of 250 nM, added during seeding. Green fluorescence was monitored using IncuCyte® software to quantify non-viable cells with compromised membrane integrity.

## Cytokine Quantification via ELISA

Cytokine levels were quantified using enzyme-linked immunosorbent assays (ELISA) following the manufacturer's protocols. CXCL10 and CXCL11 concentrations were determined using the Human CXCL10/IP-10 and CXCL11/I-TAC DuoSet® ELISA kits (R&D Systems, Cat# DY266 and DY392), while IL-2 and IFNG levels were measured using the BD OptEIA™ ELISA sets (BD Biosciences). 96-well microplates (NUNC) were coated overnight at 4°C with the respective cytokine-specific capture antibodies. After washing, plates were blocked with 10% fetal calf serum (FCS) for IL-2 and IFNG ELISAs or 1% bovine serum albumin (BSA) for CXCL10 and CXCL11 ELISAs. Frozen samples were thawed and analyzed at multiple dilution factors to ensure accurate quantification: 1:10, 1:100, or undiluted. Detection was performed using biotinylated secondary antibodies, streptavidin-HRP and TMB substrate, with signal development for 20 min at room temperature in the dark. The reaction was stopped with 2N H<sub>2</sub>SO<sub>4</sub> (50 μL/well). Absorbance was measured at 450 nm (reference: 570 nm) using an Epoch™ microplate spectrophotometer (Gene5 software). Standard curves were generated using four-parameter linear regression in Microsoft Excel.

#### Flow Cytometry and Fluorescence-Activated Cell Sorting (FACS)

Flow cytometry was used to analyze transgene expression, cell surface markers and viability, while fluorescence-activated cell sorting (FACS) was performed to enrich successfully modified cells. All flow cytometric analyses were conducted on BD FAC LSRFortessa X-20 (Lasers for Detection: 405 nm (violet), 488 nm (blue), 561 nm (yellow-green), 640 nm (red)), with sorting performed using a BD FACSAria III. Data acquisition and analysis were performed using FlowJo v10. A comprehensive list of all antibodies, fluorochromes is provided in **Supplementary Table 6** and detailed

gating strategies are illustrated in **Supplementary Figures S10**, **S19** and **S21**. Cells were collected, washed twice with PBS and resuspended in 100  $\mu$ L staining solution containing the respective fluorochrome-conjugated antibodies. For CD34-epitope detection and sorting, cells were labeled with PE-conjugated anti-CD34 monoclonal antibody (clone QBEND/10, Invitrogen, dilution 1:10) and incubated at 4°C for 30 min in the dark. For samples requiring CAR expression analysis, cells were pre-stained with anti-mouse F(ab')2 and blocked with mouse serum (MilliporeSigma) before antibody labeling. FACS was used to enrich CD34-positive genome-edited cells, ensuring a homogeneous population. Cells were harvested, stained for CD34 expression and sorted using BD FACSAria III. The sorted fraction was collected in FBS-coated tubes, resuspended in culture medium and expanded for further analyses. Fluorescence signals were compensated using single-stained CD8+ T cells.

#### Boyden chamber and Clearview trans well migration assays

The migration potential of L1CAM-specific CAR T cells was assessed using a 24-well Boyden chamber transwell system with 8  $\mu$ m pore size polycarbonate membranes. Inserts were pre-coated with 0.5% bovine serum albumin (BSA) in PBS for 1 hour at room temperature. CAR T cells were resuspended at 5 × 10<sup>6</sup> cells/mL at day 12-15 after expansion initiation seeded into the upper transwell chamber (100  $\mu$ L per well). The lower chamber contained 500  $\mu$ L of conditioned medium from cytokine-expressing neuroblastoma cells or control medium. Migration was monitored for 4 hours using the IncuCyte S3 live-cell imaging system and data were analyzed using the IncuCyte S3 software. Data were normalized to initial seeding density and analyzed using GraphPad Prism with migration parameters compared via Gompertz-Laird model fitting and statistical tests. The ClearView Transwell Migration Assay was performed using the IncuCyte ClearView Cell Migration Plate in a 96-well format with a pore size of 8  $\mu$ m. The membrane surface was coated with 1% BSA solution before being incubated with Protein G (20  $\mu$ g/mL, Thermo Fisher, #101200) for 1 hour at 37°C, followed by an additional 40  $\mu$ L wash with Protein G solution. The membrane was then coated with ICAM-1 (5  $\mu$ g/mL, Sino Biological, #10346-H03H) for 2 hours at 37°C before both sides were blocked with PBS + 1% BSA for 30 min at room temperature. CAR T cells (50,000 per well) were seeded at day 12-15 after expansion initiation in 60  $\mu$ L RPMI + 0.5% FCS and allowed to attach for 45-60 min before the addition of 200  $\mu$ L chemoattractant solution prepared in RPMI + 0.5% FCS to the lower chamber.

#### Generation of L1CAM knock-out SK-N-BE2c

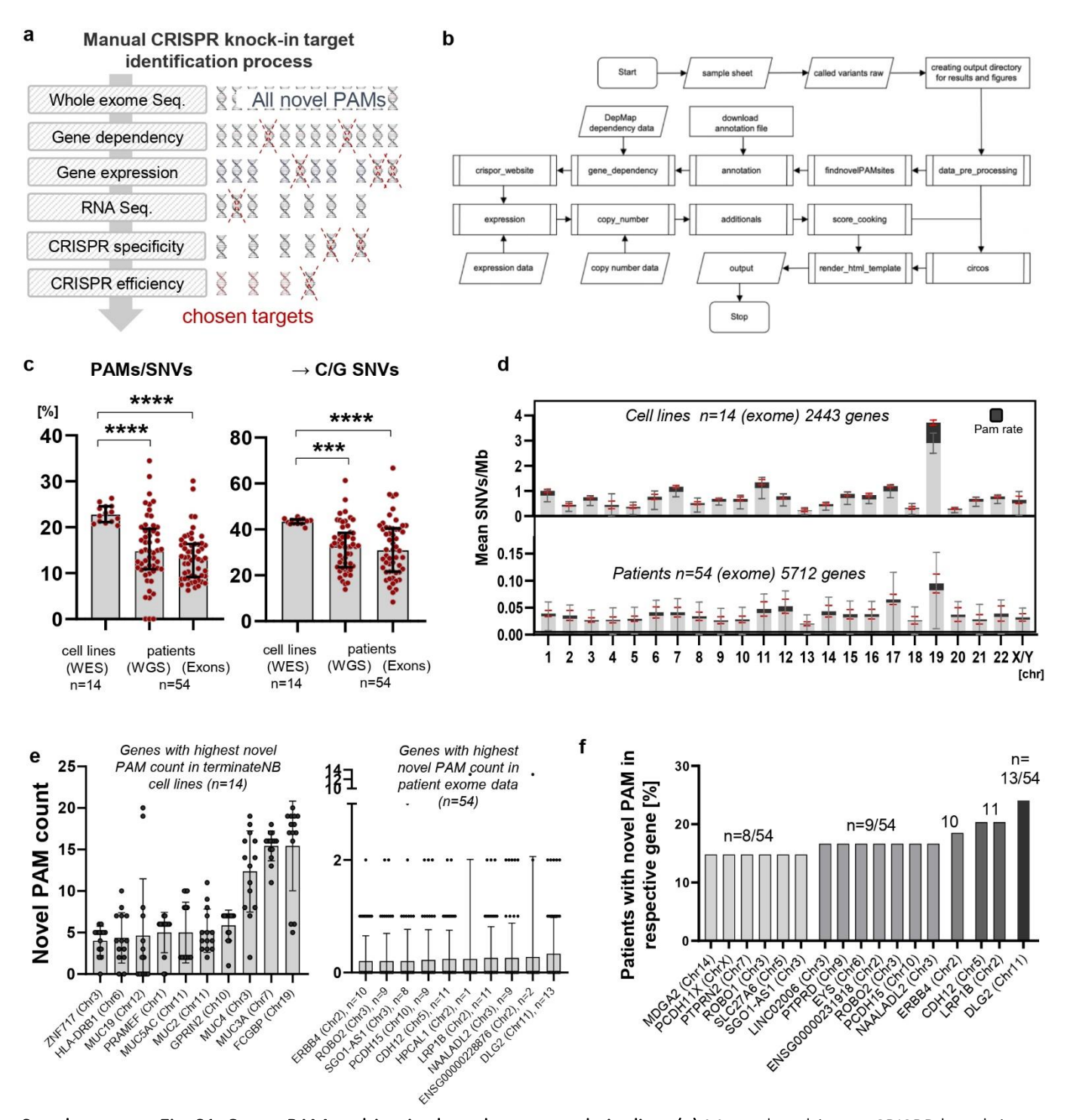
SK-N-BE2c cells were transfected with a plasmid encoding Cas9 and a L1CAM-targeting guide RNA and a puromycin resistance gene. Specifically,  $1\times10^6$  cells were seeded in a 6-well plate containing 3 mL of culture medium. The following day, the medium was replaced and cells were transfected using Effectene Transfection Reagent (QIAGEN) according to the manufacturer's protocol, utilizing 1  $\mu$ g of plasmid DNA per transfection. On day two post-transfection, the medium was refreshed and on day three, selection commenced with 0.5  $\mu$ g/mL puromycin. A control plasmid lacking the puromycin resistance gene was used as a negative control. By day ten, knockout efficiency was assessed via flow cytometry. Subsequently, to create a cell line with complete L1CAM knockout, single-cell clones were isolated and expanded.

## Immunohistochemistry (IHC)

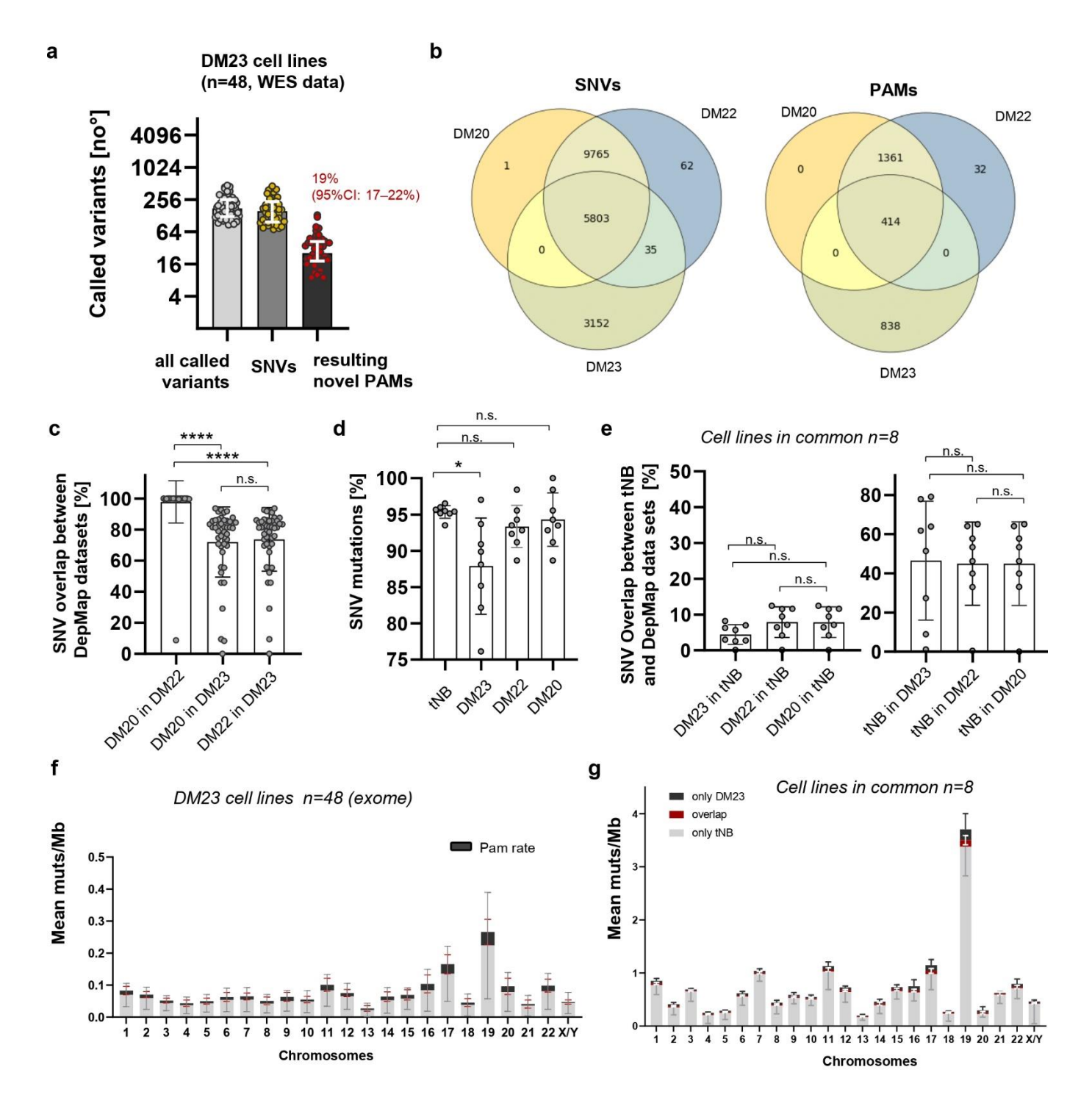
Immunohistochemistry was performed on paraffin-embedded tumor tissues. Tumors were fixed, dehydrated and embedded in paraffin before sectioning into 6 μm slices using a microtome. Sections were mounted on positively charged glass slides and subjected to deparaffinization in xylene (twice, 5 min each), followed by rehydration in a graded ethanol series (100%, 95%, 70% and 50% ethanol, 5 min each) and rinsing in distilled water. Antigen retrieval was performed in citrate buffer (10 mM tri-sodium citrate, 0.05% Tween-20, pH 6.0, Abcam ab93678) using a pressure cooker (2 min at 125°C, cooling to 90°C, then under running water for 10 min). After an additional 5 min incubation in distilled water, sections were washed in PBS (5 min). To prevent non-specific binding, blocking was performed using 3% normal serum (corresponding to the species of the secondary antibody) in TBS-T for 1 hour in a humidity chamber. For immunofluorescence staining, primary antibodies were applied in 3% serum in TBS-T and incubated overnight at 4°C. The following primary antibodies were used: rabbit anti-human/mouse CD3 (Abcam, ab16669, clone SP7, 1:100), mouse anti-human L1CAM (Invitrogen, MA1-46044, clone UJ127.11, 1:500). The next day, slides were washed five times in TBS-

T before incubation with fluorescently labeled secondary antibodies in TBS-T and 3% serum for 1 hour at room temperature. The following secondary antibodies were used: donkey anti-rabbit Alexa 594 (Invitrogen, Lot# 1938375, 1:300), donkey anti-mouse Alexa 488 (Invitrogen, Lot# 1975519, 1:300), goat anti-rabbit Alexa 594 (Invitrogen, 1:500), goat anti-mouse Alexa 488 (Invitrogen, Lot# A11001, 1:500). Following secondary antibody incubation, slides were washed 3 times in TBS-T and counterstained with Hoechst (1:2000 in TBS-T, 2–5 min). After a final wash in distilled water (5 min), samples were mounted using Eukitt quick-hardening mounting medium (Sigma-Aldrich, Lot# BCBP7505V). Immunofluorescence images were acquired using a fluorescence microscope (Olympus BX43) and analyzed with Olympus cellSens software.

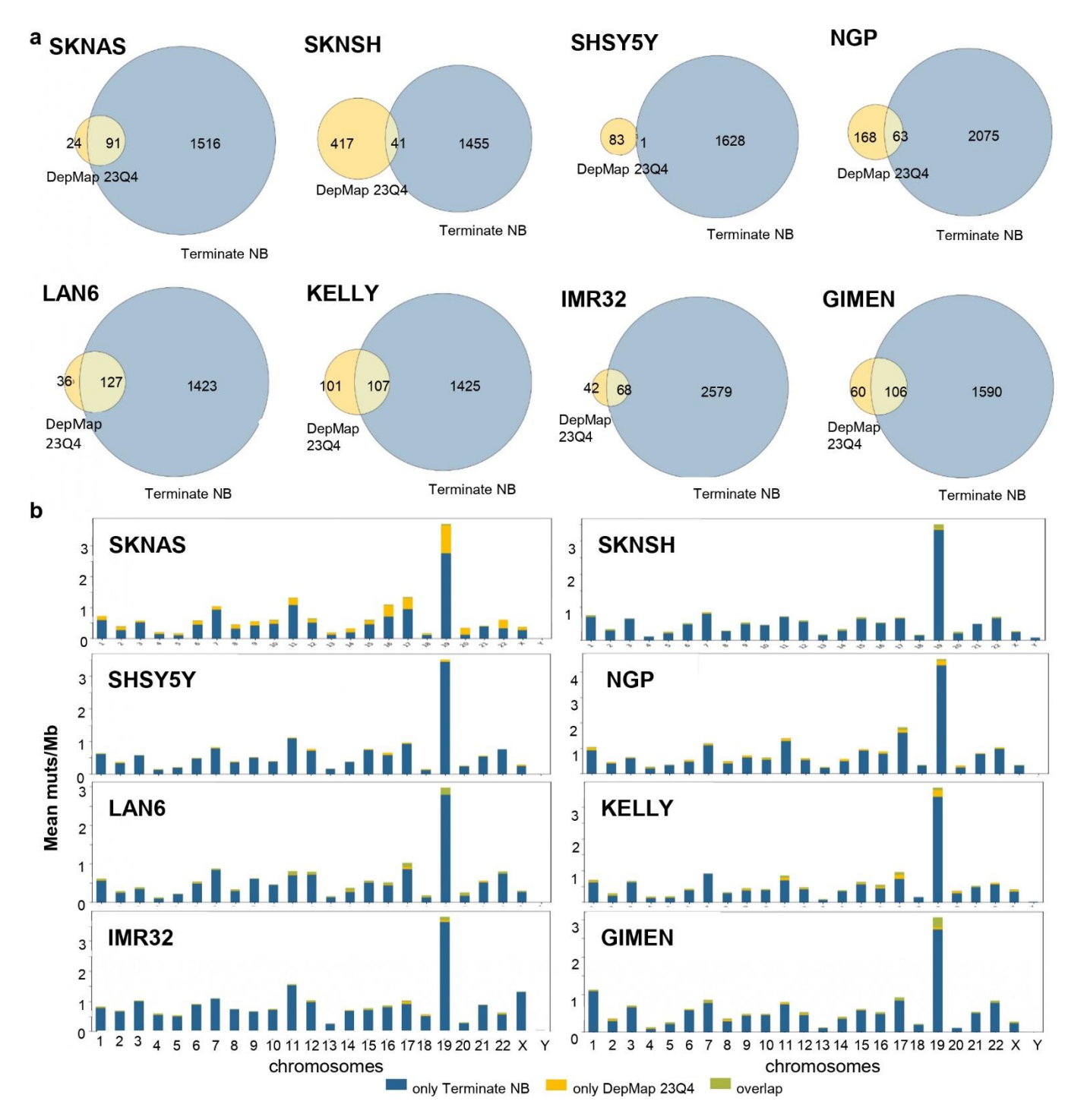
## Supplementary Figures



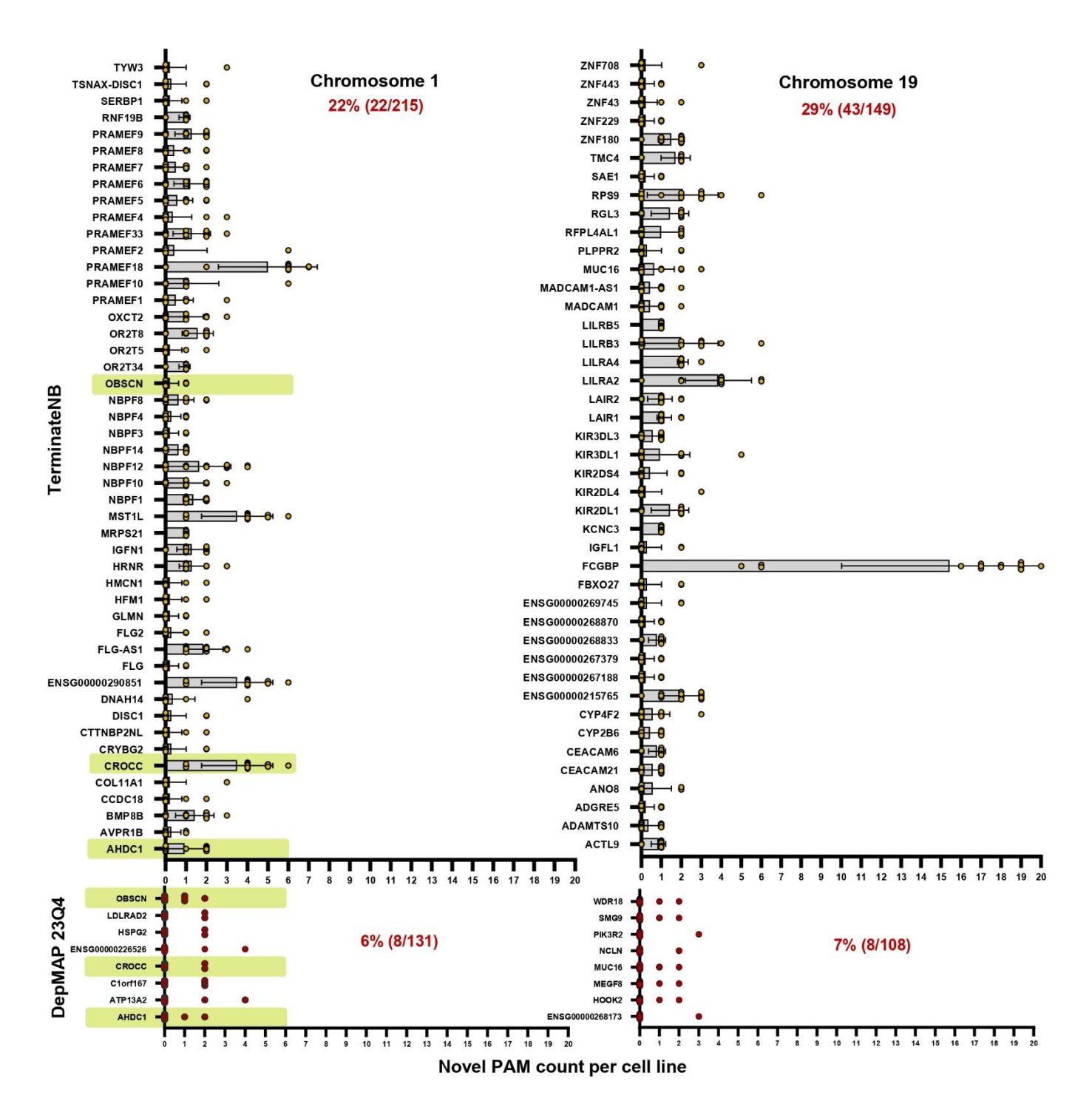
Supplementary Fig. S1. CancerPAM multiomics-based automated pipeline. (a) Manual multi-step CRISPR knock-in target identification process preceding the CancerPAM pipeline, where novel PAM sites were excluded as potential targets if they fell below defined threshold values at each step. (b) Visualization of the CancerPAM pipeline data flow. (c) Comparison of the proportion of novel PAMs within all SNVs and mutations to C or G ( $\rightarrow$  C/G) in cell line versus patient data. (d) Chromosomal distribution of exonic mutations in neuroblastoma cell lines and patient samples(F-H) Proportion of patients with novel PAM counts in the same gene, focusing on the 16 genes most frequently recurring across patients. (e) Quantification of novel PAM counts in the top 10 genes with the highest novel PAM counts in cell line or patient data. (f) Proportion of patients with novel PAM counts in the same gene, focusing on the 16 genes most frequently recurring across patients. Data presentation: (c,d) Means  $\pm$  SD. Statistical analysis: (c) Kruskal-Wallis with Dunn's post hoc test. p values: \*<0.05, \*\*<0.01, \*\*\*<0.001, \*\*\*\*<0.0001; n.s.: not significant.



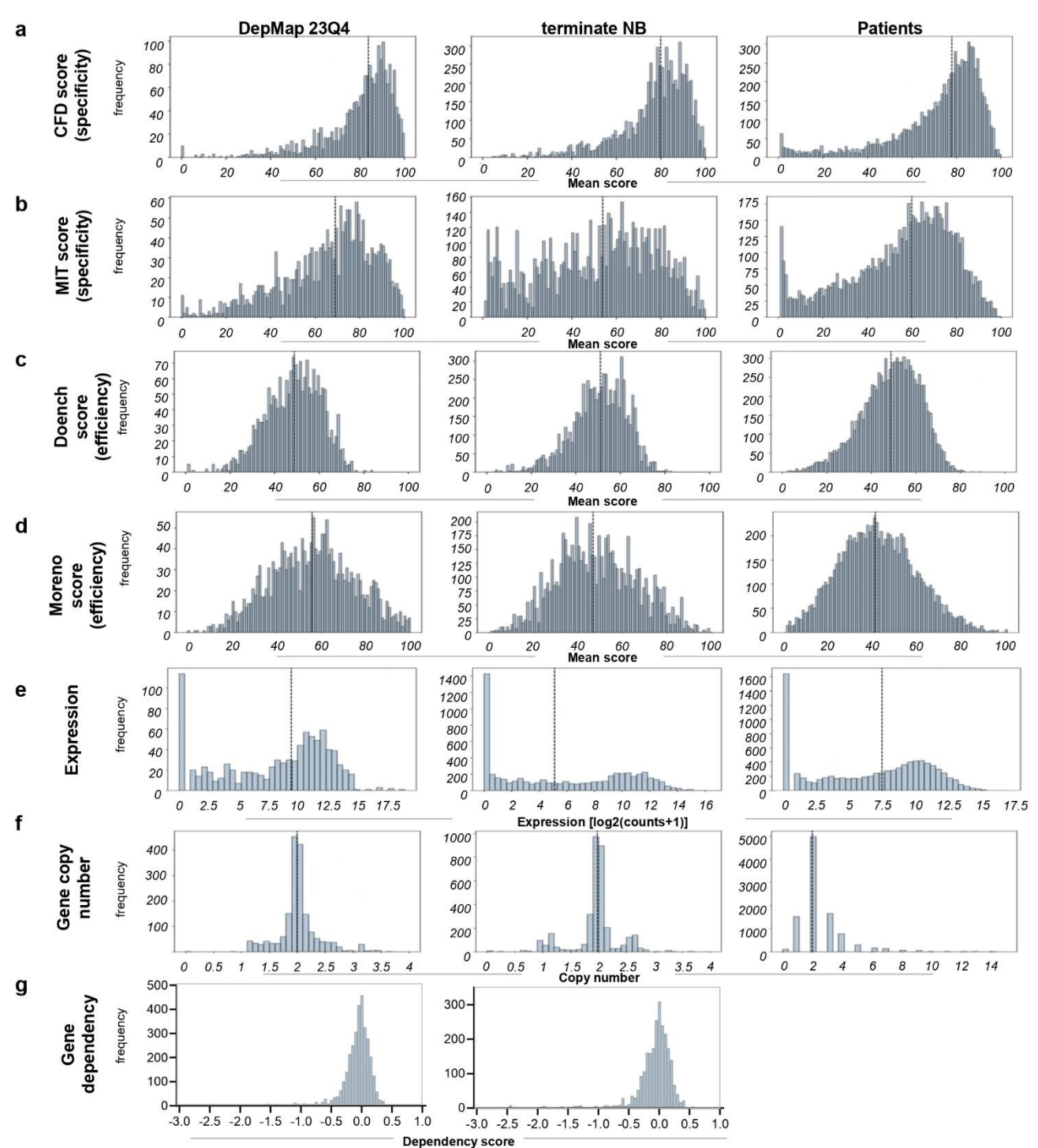
Supplementary Fig. S2. Dataset comparison between Terminate NB and DepMap. (a) Quantification of identified variants and tumor-specific PAM sites in neuroblastoma cell lines from the DepMap 23Q4 (DM23) dataset (WES data) identified using the CancerPAM pipeline. (b) Overlap of SNVs and novel PAMs identified in neuroblastoma cell lines across the three DepMap datasets: DepMap 20Q4 (DM20), DepMap 22Q2 (DM22) and DepMap 23Q4 (DM23). (c) Overlap of identified SNVs between DepMap datasets, where bars represent the percentage of SNVs in the first dataset that were also found in the second dataset. (d) Comparison of the percentage of identified SNVs between terminate NB (tNB) and DepMap datasets. (e) Overlap of identified SNVs between terminate NB and DepMap datasets for all cell lines present in all datasets, with bars showing the percentage of SNVs in the first dataset also identified in the second dataset. (f) Chromosomal distribution of exonic mutations in neuroblastoma cell lines from the DM23 dataset. (g) Overlap of identified SNVs and novel PAMs between terminate NB and the DM23 dataset per chromosome. Data presentation: (a,d-e) Means ± SD. Statistical analysis: (c-e) Kruskal-Wallis with Dunn's post hoc test; p values: \*<0.05, \*\*<0.01, \*\*\*\*<0.001; n.s.: not significant.



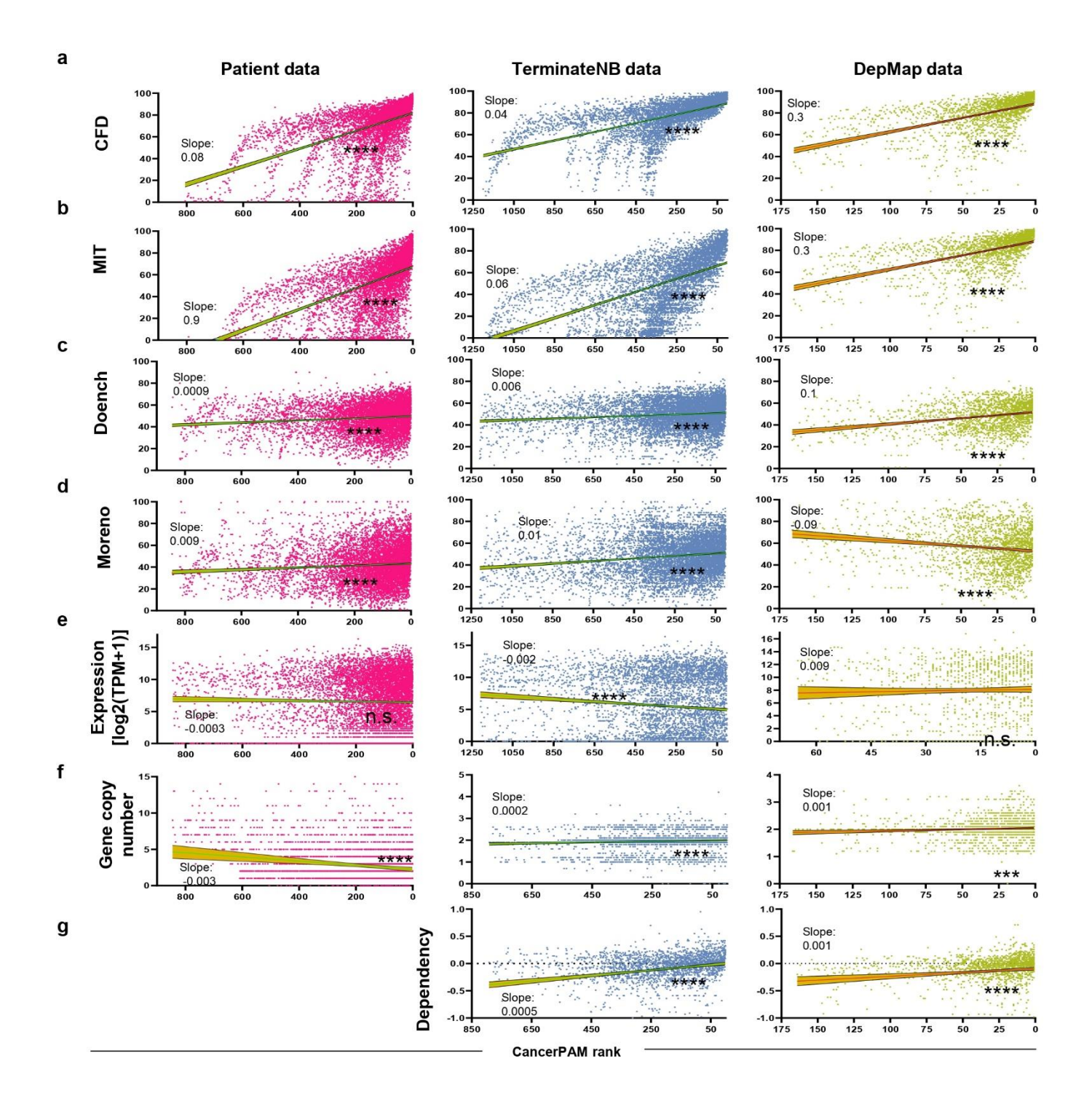
Supplementary Fig. S3. Cell line data comparison between Terminate NB and DepMap data sets. (a) Overlap of SNVs identified in neuroblastoma cell lines across the terminate NB and DepMap 23Q4 data sets. (b) Overlap of identified SNVs and novel PAMs between terminate NB and the DepMap 23Q4 dataset per chromosome for all cell lines included in both data sets.



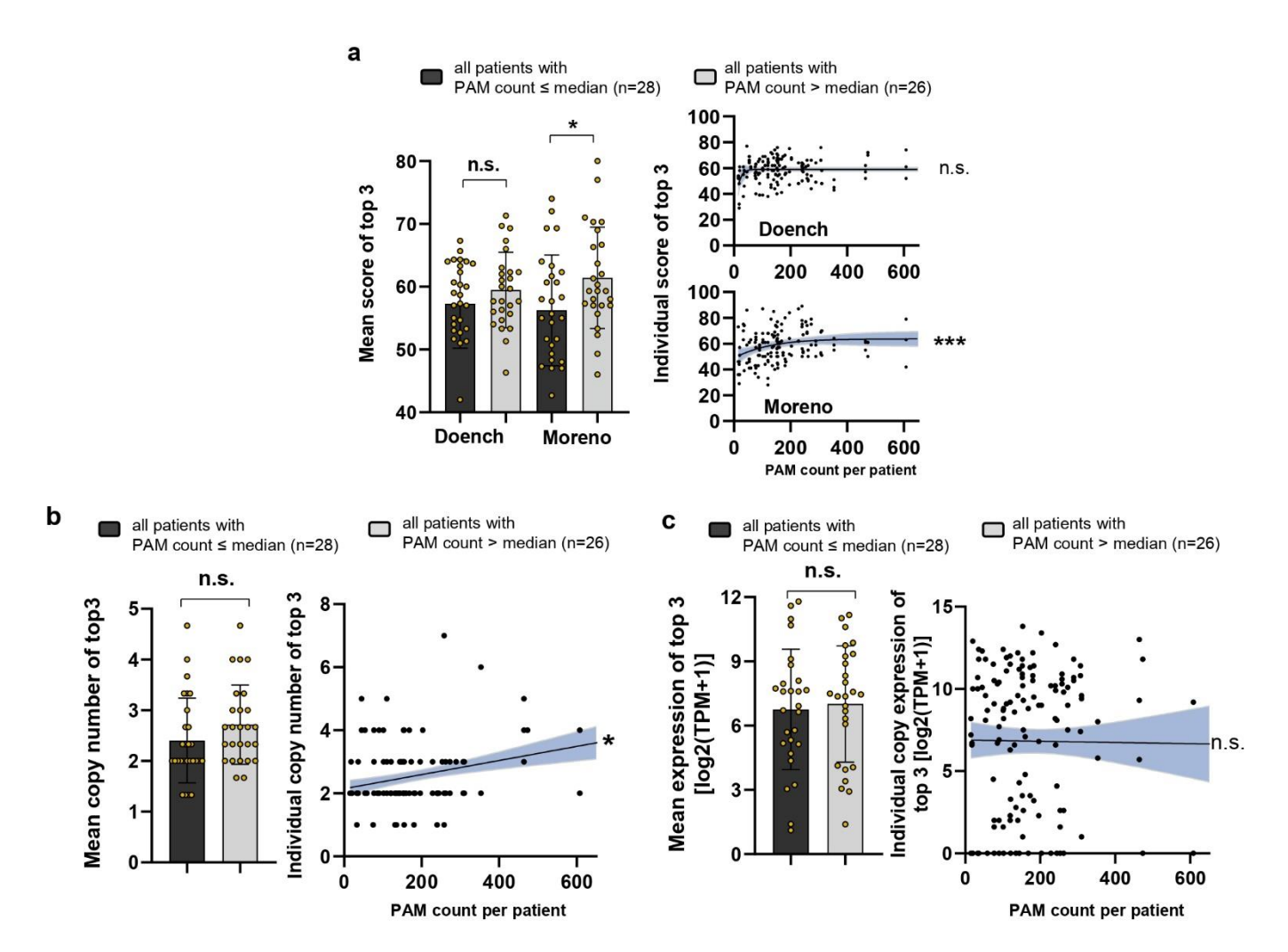
Supplementary Fig. S4. Chromosomal novel PAM distribution. Visualization of all genes with at least two novel PAMs on Chromosomes 1 and 19 found in at least one cell line from the terminate NB cell line dataset (n = 14) and the DepMap 23Q4 dataset (n = 48). In the terminate NB dataset, 22% (22/215) and 29% (43/149) of the genes on Chromosomes 1 and 19, respectively, with novel PAMs contained at least two novel PAMs in at least one analyzed cell line. For the DepMap 23Q4 dataset, this proportion was 6% (8/131) and 7% (8/108) for Chromosomes 1 and 19, respectively. Green bars indicate genes with at least two novel PAMs in at least one cell line that were shared between both datasets.



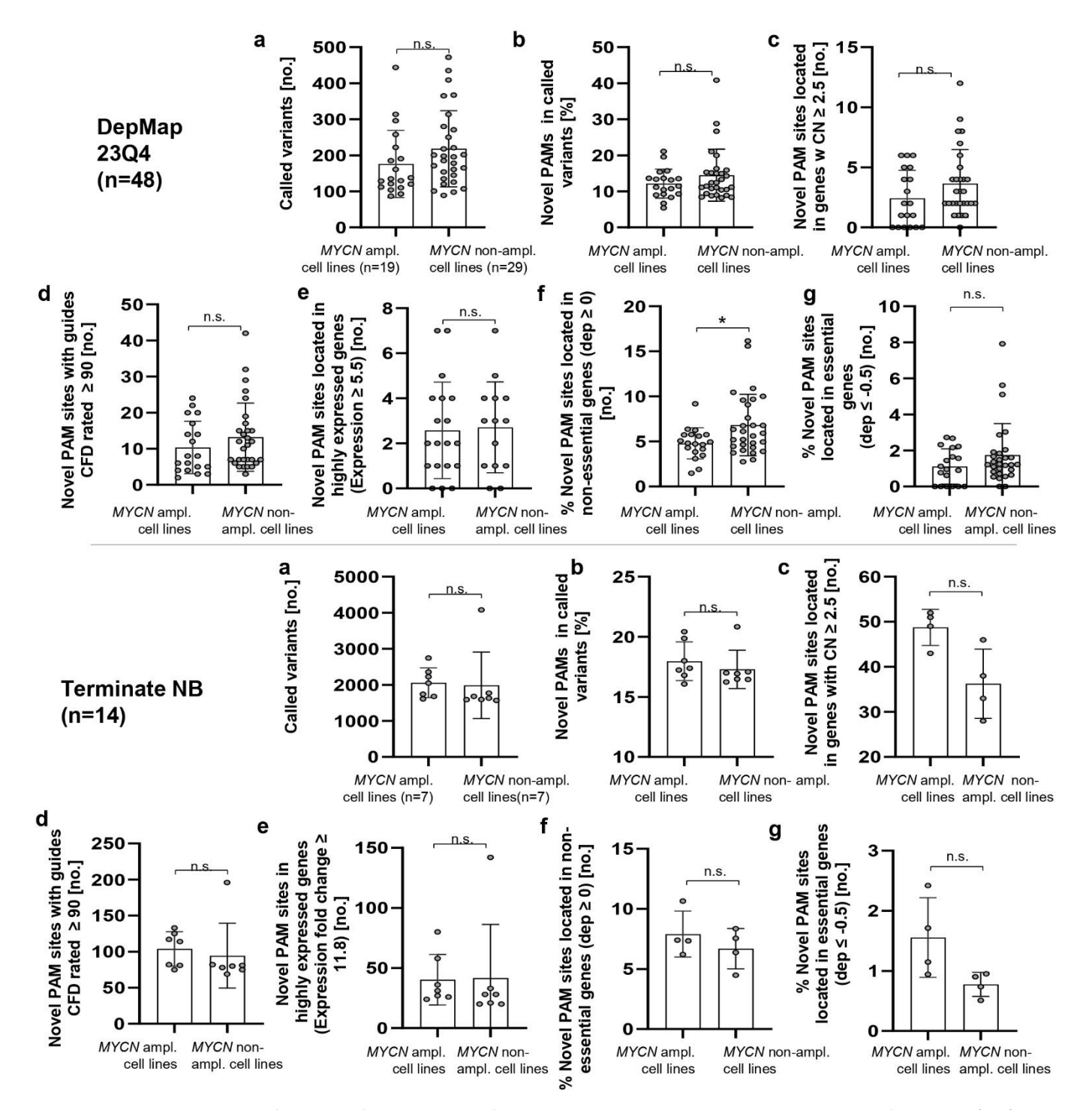
Supplementary Fig. S5. Novel PAM feature characteristics distribution. (a-g) Frequency distribution of values for various features annotated to the identified novel PAM sites in the DepMap 23Q4, terminate NB and patient datasets. The DepMap 23Q4 dataset includes data from 48 cell lines, terminate NB includes 14 cell lines and the patient dataset consists of 54 patients. Analyzed features include the CRISPR specificity scores CFD (a) and MIT (b), the CRISPR efficiency scores Doench (c) and Moreno (d), as well as gene expression levels (e), copy number (f) and Gene dependency scores (g) associated with novel PAM sites.



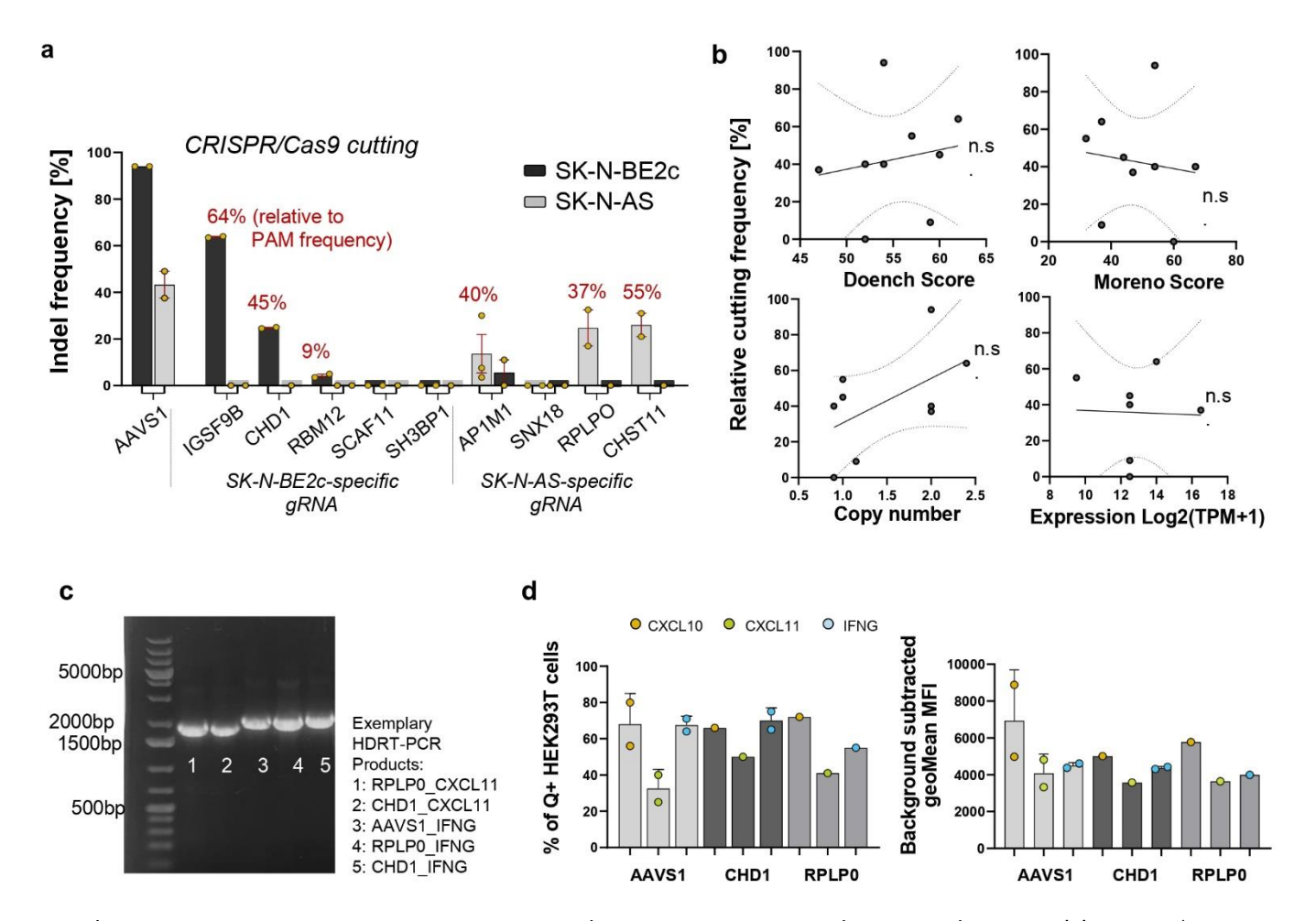
Supplementary Fig. S6. CancerPAM ranking validation. (a-g) Correlation analysis of novel PAM feature values against the CancerPAM rank of the identified novel PAM sites. Analyzed features include the CRISPR specificity scores CFD (a) and MIT (b), the CRISPR efficiency scores Doench (c) and Moreno (d), gene expression levels (e), copy number (f) and DepMap gene dependency (g, not available for patient data) from genes associated with the novel PAM sites. Statistical analysis: Linear regression for curve fitting and slope calculation, followed by Spearman correlation analysis. p values: \*<0.05, \*\*<0.01, \*\*\*<0.001; n.s.: not significant.



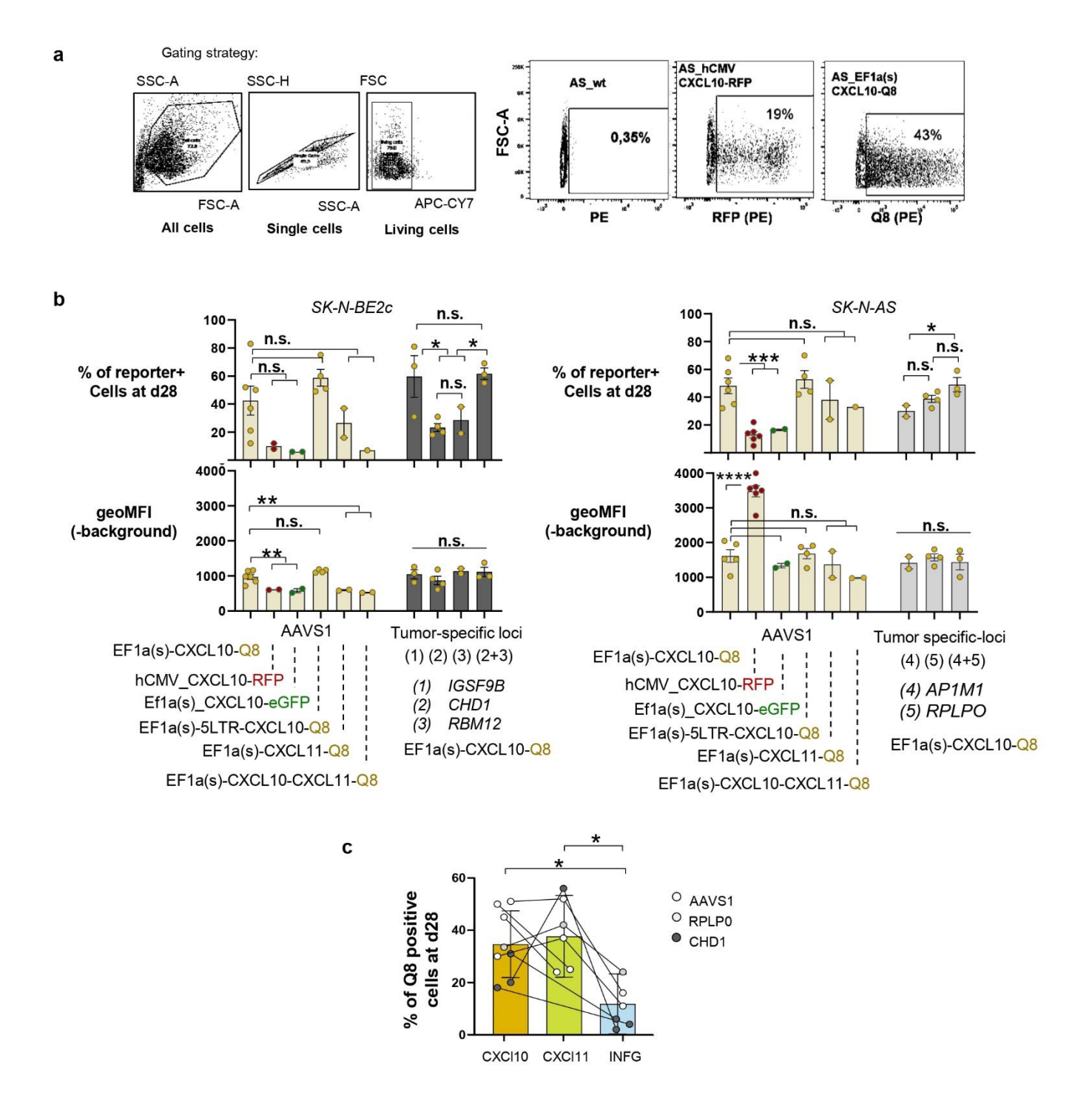
Supplementary Fig. S7. Feature correlation with PAM count. (a-c) Bar graphs comparing patients with a high (>median; n = 26) versus low ( $\leq$ median; n = 28) PAM count in terms of the top three ranked PAM mean Doench and Moreno efficiency scores (a), copy number (b), or expression levels (c) X/Y scatter plots depict the correlation of individual scores for the top three ranked novel PAM sites across patients (n = 162) against total tumor-specific PAM counts per patient. Data presentation: (a-c) Means  $\pm$  SD. Statistical tests: (a-c) Bar graphs: Kruskal-Wallis with Dunn's post hoc test; X/Y scatter plots: logistic and linear regression for curve fitting and Spearman correlation. p values: \*<0.05, \*\*<0.01, \*\*\*\*<0.001; n.s.: not significant.



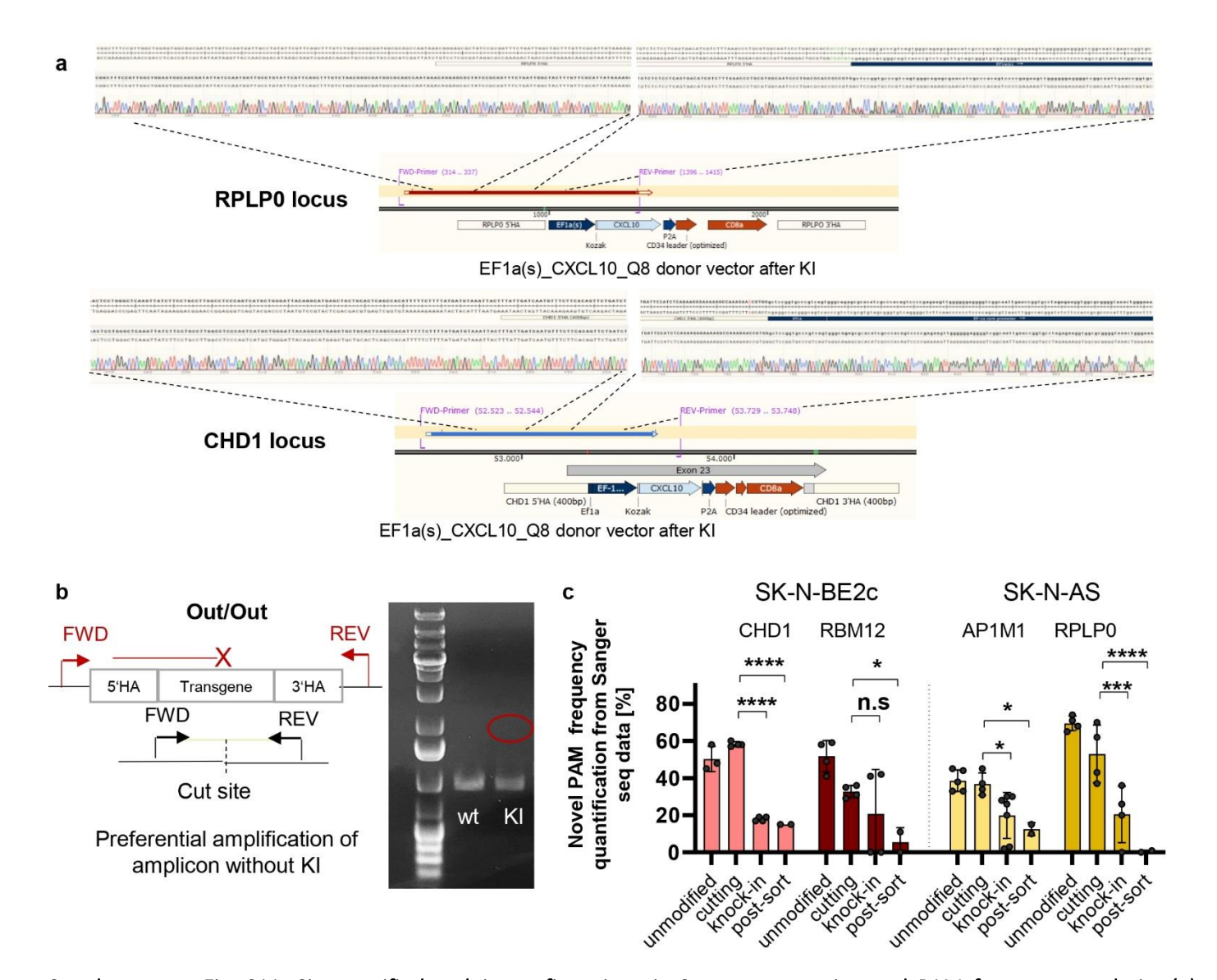
Supplementary Fig. S8. Influence of MYCN amplification status on novel PAM counts and features. (a-g) Group comparisons of novel PAM counts and feature values between MYCN-amplified and non-amplified cell lines for the terminate NB and DepMap 23Q4 datasets. Comparisons include the number of called variants per cell line (a), the percentage of novel PAMs among all called variants (b), the number of novel PAMs located in genes with a copy number (CN)  $\geq$  2.5 (c), the number of novel PAM sites with guides showing a CFD score  $\geq$  90 (d), the number of novel PAM sites located in highly expressed genes with log2(counts+1)  $\geq$  5.5 (e), the number of novel PAM sites located in non-essential genes with gene dependency (dep) values  $\geq$  0 (f) and the number of novel PAM sites located in essential genes with gene dependency (dep) values  $\leq$  -0.5 (g). Data presentation: (a-g) Means  $\pm$  SD. Statistical analysis: (a-g): Mann-Whitney test. p values: \*<0.05, \*\*<0.01, \*\*\*<0.001; n.s.: not significant.



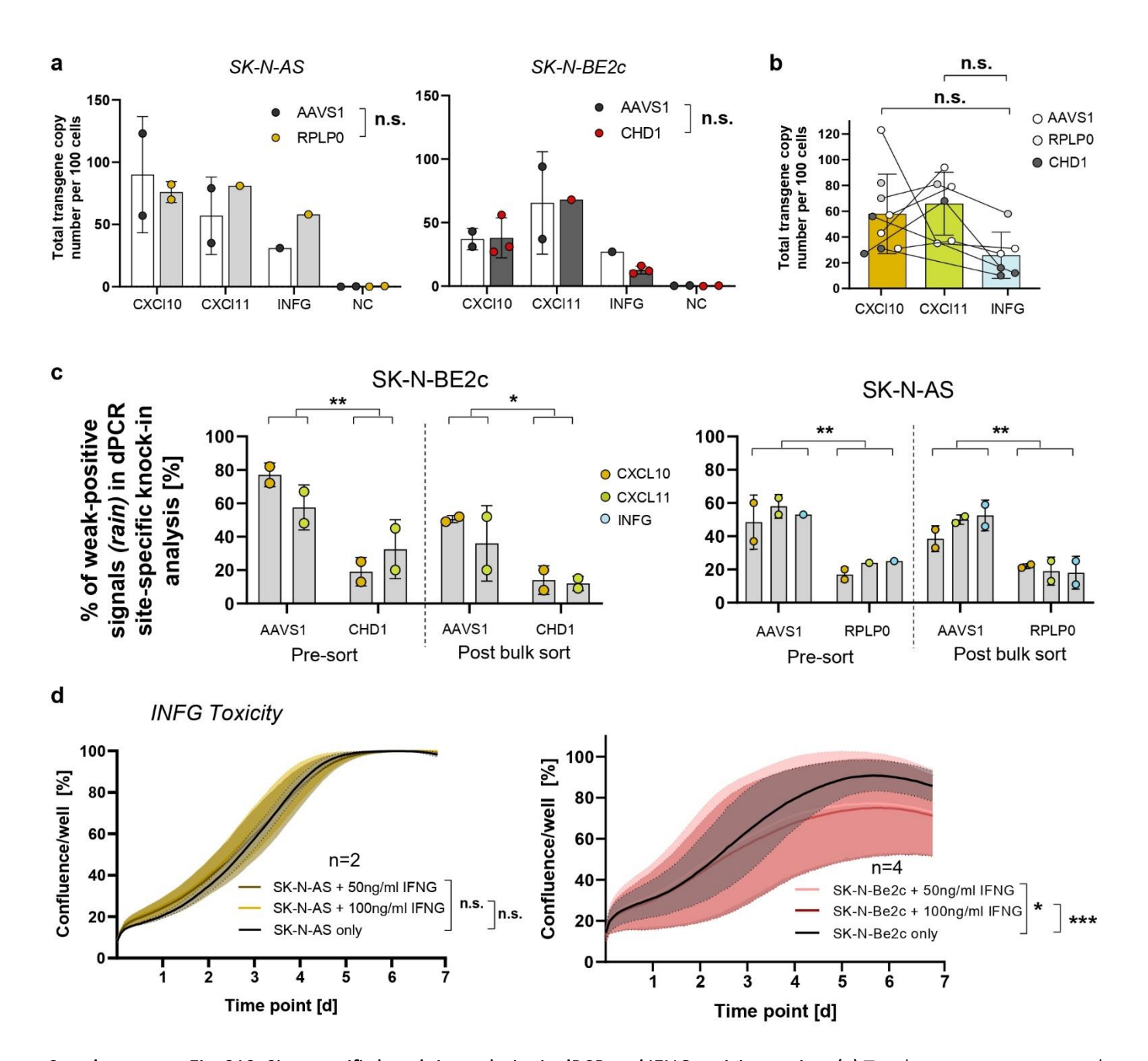
Supplementary Fig. S9. In vitro CRISPR cutting and transgene vector production and testing. (a) CRISPR/Cas9 cutting efficiency at the chosen target sites and the AAVS1 control locus, represented by indel frequency determined via Sanger sequencing and Synthego ICE analysis. (b) Correlation between relative cutting frequency (INDEL% / target site frequency) and the CRISPR efficiency scores (Doench and Moreno), as well as target gene copy number and expression. (c) Exemplary DNA gel electrophoresis result after homology directed repair template (HDRT) production using PCR and bead-based clean up. (d) Transgene expression from the produced HDRTs as represented by the percentage of positive cells and mean fluorescence intensity (MFI) in a preliminary vector expression test using HEK293T cells and the Effectene transfection reagent. Data presentation: (a, d) Means ± SD. Statistical analysis: (e) Linear regression for curve fitting and Spearman correlation. n.s., not significant.



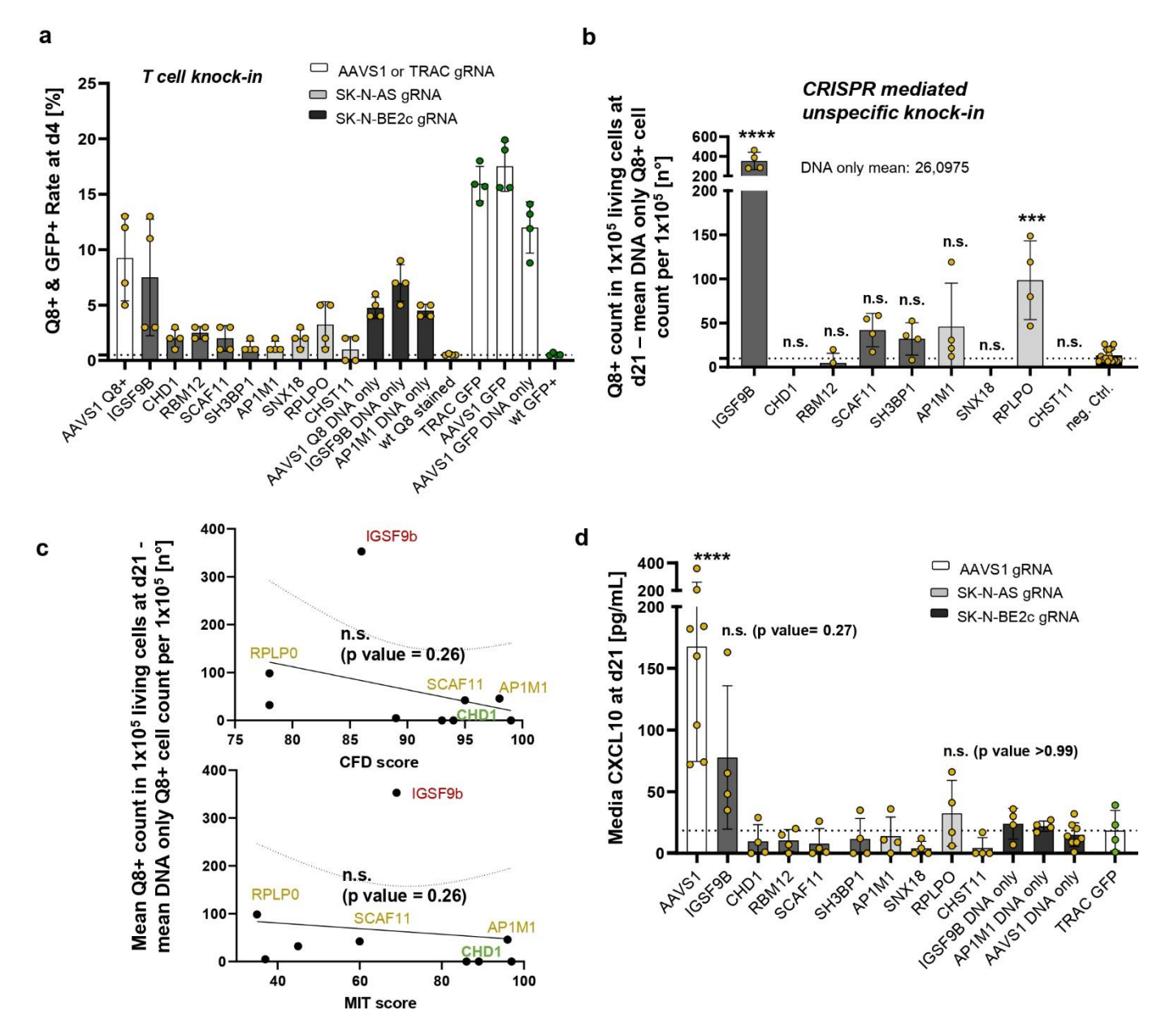
Supplementary Fig. S10. In vitro CRISPR knock-in. (a) Exemplary flow cytometry analysis and gating strategies of tumor cell lines 28 days after RNP + dsDNA template electroporation. Q8 reporter positivity was measured using PE-labeled CD34 Monoclonal Antibody QBEND/10 (Thermo Fisher). (b) Knock-in rates (%) and reporter expression strengths, represented by background-subtracted geometric mean fluorescence intensity (geoMFI), 28 days post-CRISPR KI for different constructs and loci in SK-N-BE2c and SK-N-AS neuroblastoma cell lines. Compared promoters include human CMV and a custom EF1a-derived promoter with or without a lentivirus-derived 5′ long terminal repeat (LTR) sequence. HDRT templates were designed for cytokines with a Q8 reporter and for CXCL10 with red (RFP) or green fluorescent protein (GFP) reporters. Additional tests included a tri-cistronic vector with two cytokines and a combinatorial knock-in using two HDRTs (differing homology arms) and guide RNAs (two tumor-specific loci) simultaneously without increasing total DNA or gRNA dose. In SK-N-BE2c, CHD1 and RBM12 were targeted; in SK-N-AS, AP1M1 and RPLPO. (c) Cumulative knock-in rate comparison for cytokine transgenes across three loci: AAVS1 (SK-N-BE2c and SK-N-AS), CHD1 (SK-N-BE2c only) and RPLPO (SK-N-AS only). Data presentation: (b, c) Means ± SD. Statistical analysis: (b) Kruskal-Wallis with Dunn's post hoc test; (c) Mixed-effects analysis with Tukey's multiple comparison test. p values: \*<0.05, \*\*<0.01, \*\*\*<0.001; n.s., not significant.



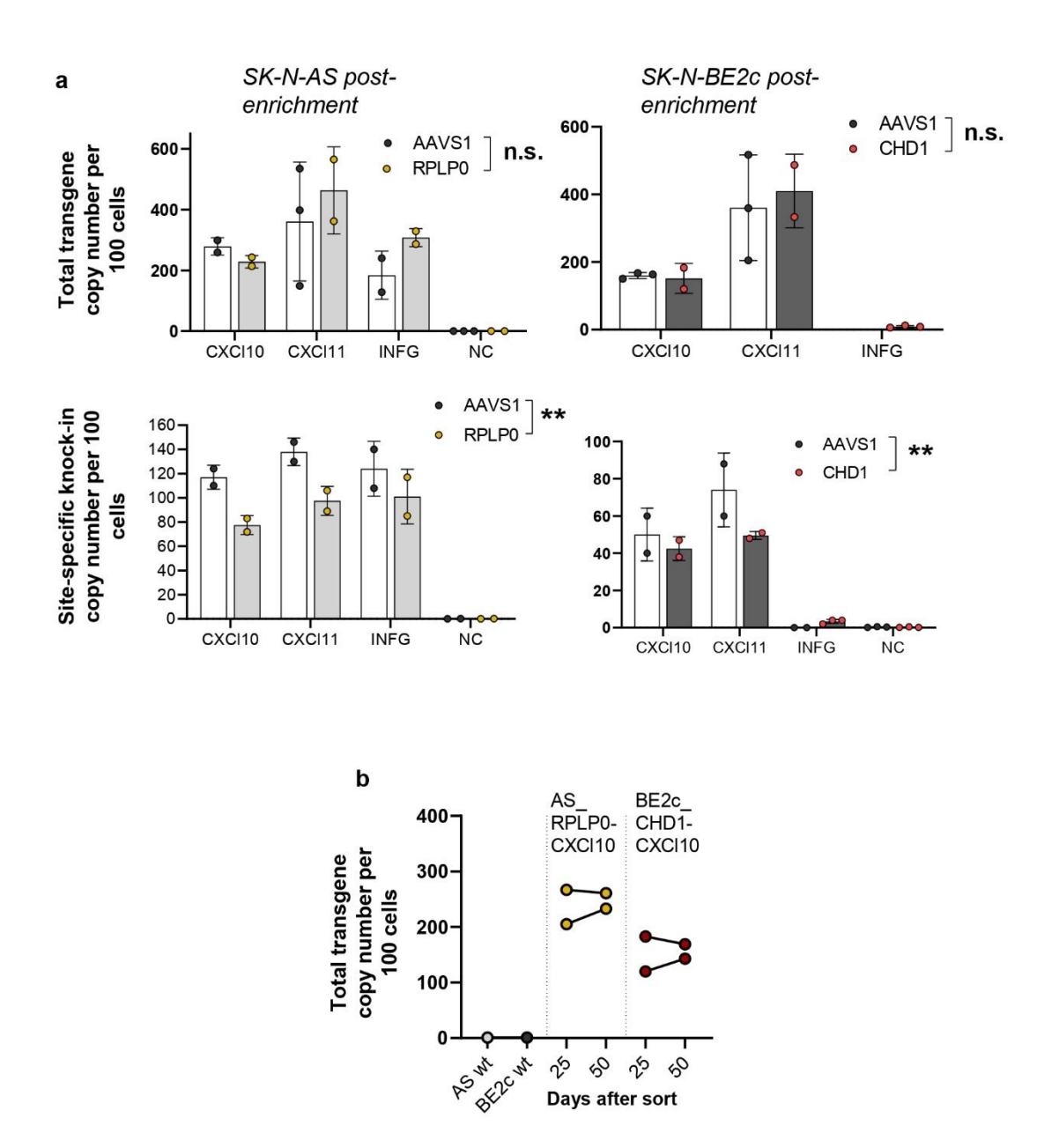
Supplementary Fig. S11. Site-specific knock-in confirmation via Sanger sequencing and PAM frequency analysis. (a) Schematic representation of on-target knock-in confirmation of an EF1a(s)\_CXCL10\_Q8 donor vector via PCR and Sanger sequencing with sequence alignment using SnapGene at the RPLPO (SK-N-AS) and CHD1 (SK-N-BE2c) loci. (b) Schematic illustrating the preferential amplification of the non-knock-in amplicon using an Out/Out PCR, where forward and reverse primers are located upstream and downstream of the homology arms and cut site, complemented by representative gel electrophoresis results. (c) Quantification of novel PAM frequency from Sanger sequencing data using EditR at the CHD1, RBM12, AP1M1 and RPLPO loci in SK-N-BE2c and SK-N-AS cell lines. Data are shown for unmodified cells, cells treated with RNP only (cutting), and cells treated with RNP+HDRT (knock-in), with or without enrichment for reporter-positive cells. Data presentation: (c) Means ± SD. Statistical analysis: (c) Two-way ANOVA with Dunnets post hoc test. p values: \*<0.05, \*\*<0.01, \*\*\*<0.001, \*\*\*\*<0.0001; n.s., not significant.



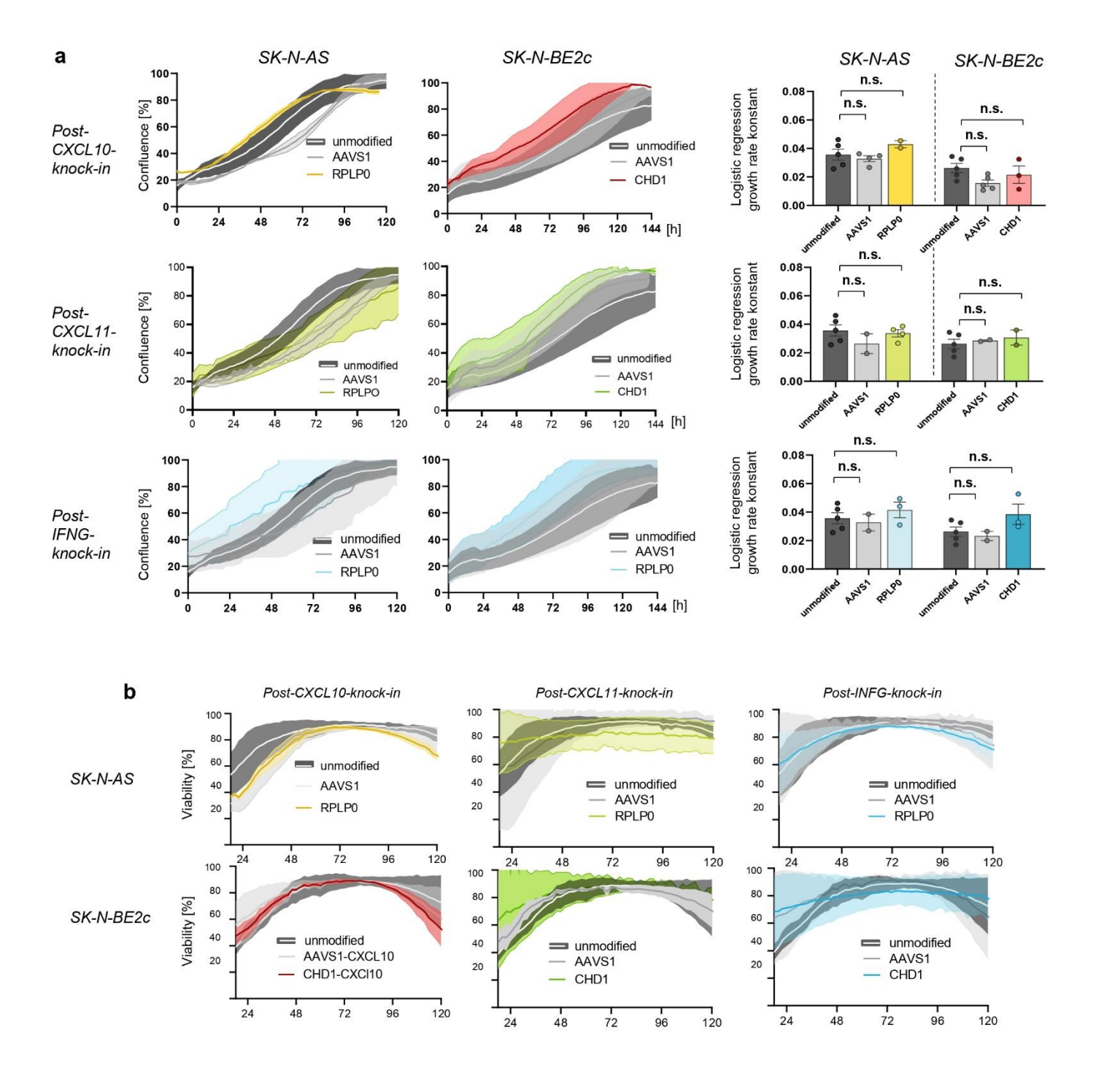
Supplementary Fig. S12. Site-specific knock-in analysis via dPCR and IFNG toxicity testing. (a) Total transgene copy number per 100 cells, 7 days after RNP/HDRT electroporation in SK-N-AS and SK-N-BE2c cell lines for different transgenes and target loci. (b) Paired analysis of cumulative total transgene copy number for the different cytokine transgenes CXCL10, CXCL11, IFNG. (c) Quantification of weak-positive signals ("rain") in digital PCR (dPCR) Out/In site-specific knock-in analysis for SK-N-BE2c and SK-N-AS neuroblastoma cell lines after HDRT knock-in at the AAVS1 control locus or novel PAM sites, before and after enrichment for reporter-positive cells.. (d) 7 day growth curves of unmodified SK-N-AS and SK-N-BE2c cell lines cultivated with varying concentrations of IFNG represented by confluence development recorded using Incucyte live imaging. Data presentation: (a-d) Means ± SD. Statistical analysis: (a-d) Two-Way-ANOVA with Tukey test. p values: \*<0.05, \*\*<0.01, \*\*\*<0.001, \*\*\*\*<0.0001; n.s., not significant.



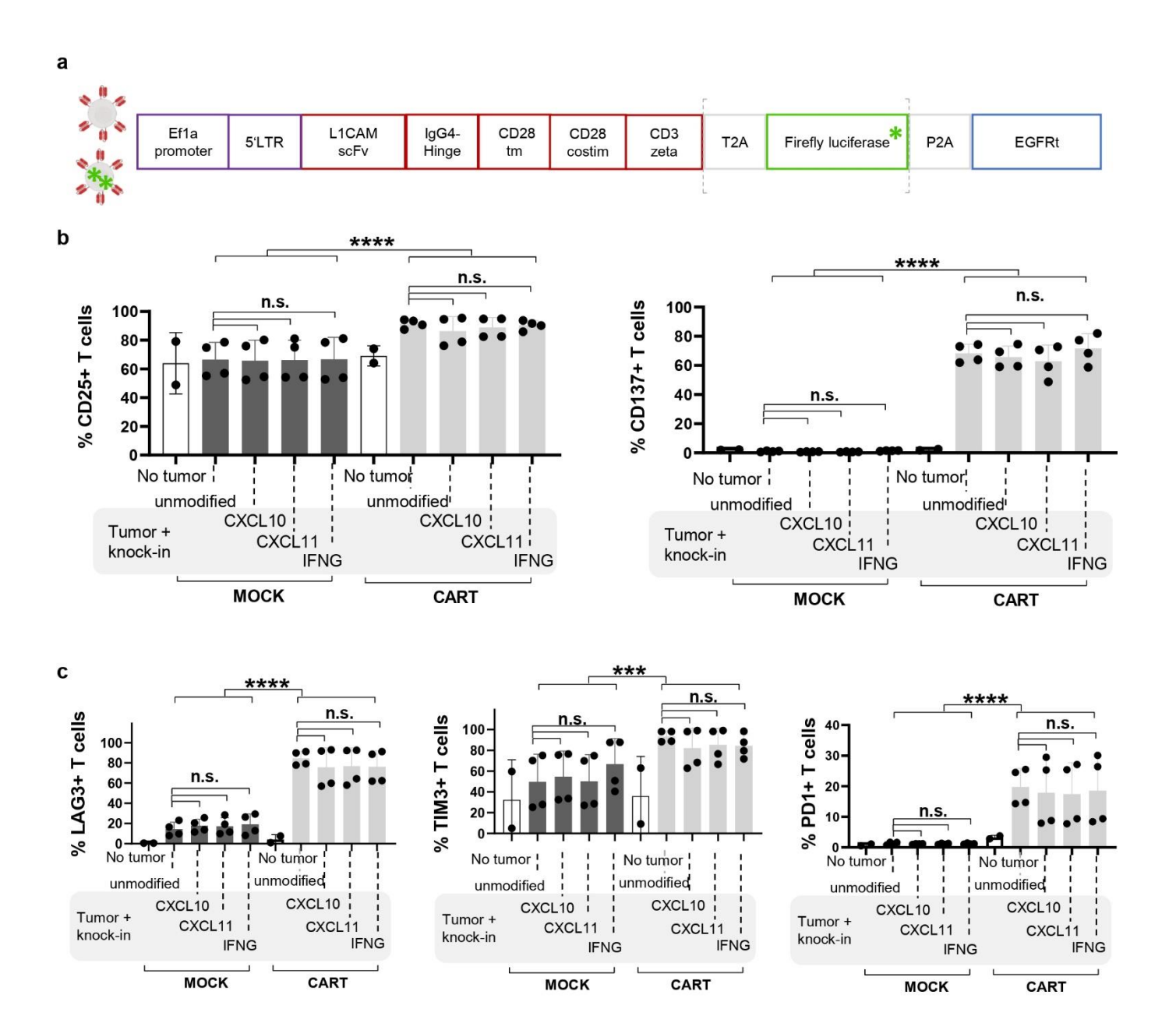
Supplementary Fig. S13. Unspecific T cell knock-in. (a) Comparison of the percentage of reporter (Q8/GFP)-positive cells 4 days after RNP/HDRT electroporation in primary T cells from two donors using gRNAs targeting neuroblastoma-specific novel PAM sites or AAVS1 and TRAC control loci, measured via flow cytometry. (b) Analysis and comparison of CRISPR-mediated unspecific knock-in rates, calculated as the Q8\* count per 100,000 cells minus the mean Q8\* count per 100,000 cells in DNA-only control samples, via high-throughput flow cytometry (>300,000 cells analyzed per sample) for Q8-reporter harboring HDRTs targeted at neuroblastoma-specific PAM sites. (c) Correlation of the mean CRISPR-mediated unspecific T cell knock-in rates, analyzed via high-throughput flow cytometry and DNA-only background subtraction (b), with CRISPR efficiency scores (CFD and MIT). (d) Quantification of secreted CXCL10 two days after media change at day 21 post-RNP/HDRT electroporation in primary T cells from two donors using gRNAs targeting neuroblastoma-specific novel PAM sites or AAVS1 and TRAC control loci via ELISA. Data presentation: (a,b,d) Means ± SD. Statistical analysis: (b,d) Kruskal-Wallis with Dunn's post hoc test; (c) Linear regression for curve fitting and Spearman correlation. p values: \*<0.05, \*\*<0.01, \*\*\*<0.001, \*\*\*\*<0.0001; n.s., not significant.



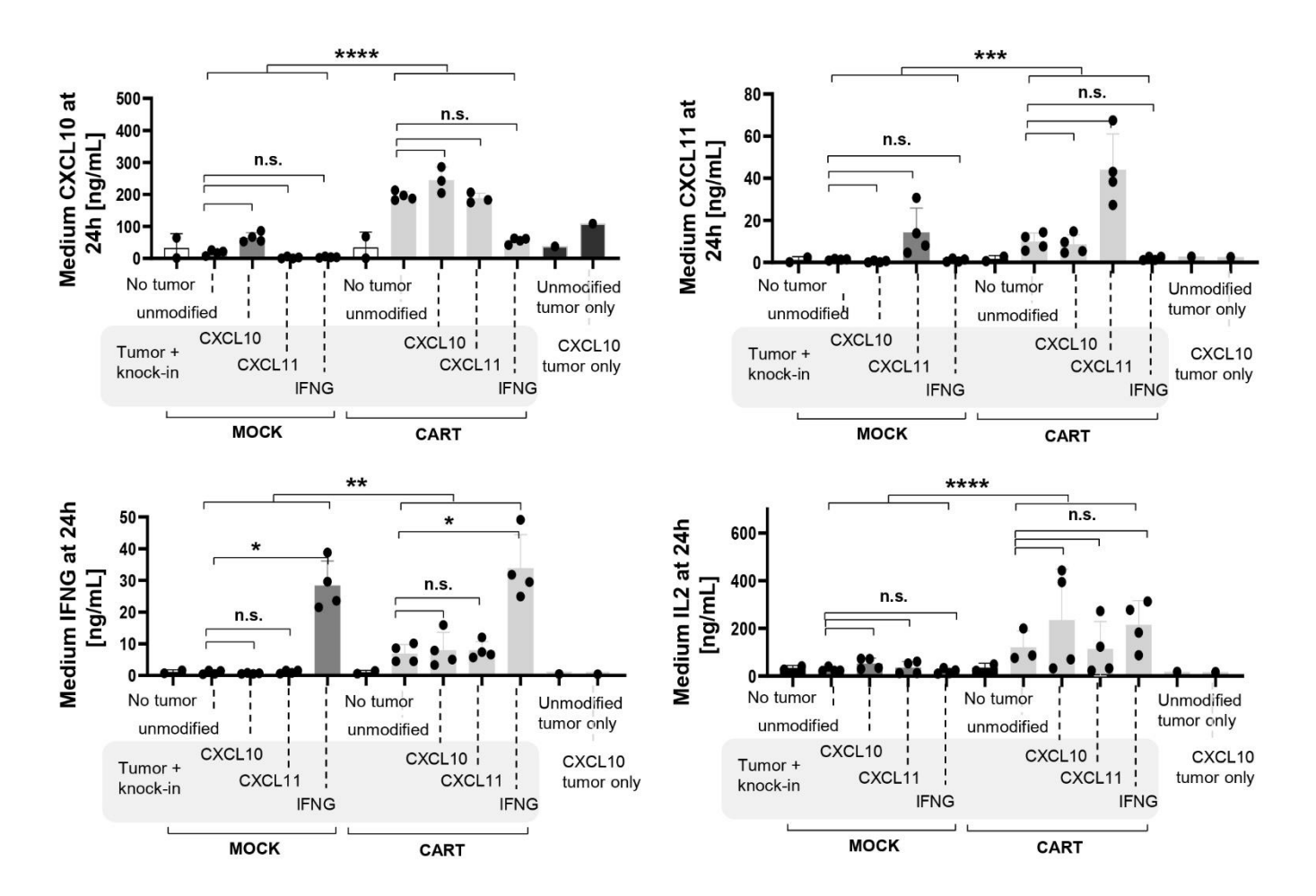
Supplementary Fig. S14. dPCR analysis after FACS enrichment. (a) Total transgene copy number and site-specific knockin copy number per 100 cells after enrichment of SK-N-AS and SK-N-BE2c knock-in cell lines for different transgenes and target loci, determined via digital PCR (dPCR). (b) Total transgene copy number 25 and 50 days after enrichment in SK-N-AS CXCL10 RPLPO and SK-N-BE2c CXCL10 CHD1 knock-in cell lines. *Data presentation:* (a) *Means ± SD. Statistical tests:* (a) *Two-way ANOVA. p values: \*<0.05, \*\*<0.01, \*\*\*<0.001, \*\*\*\*<0.0001; n.s.: not significant.* 



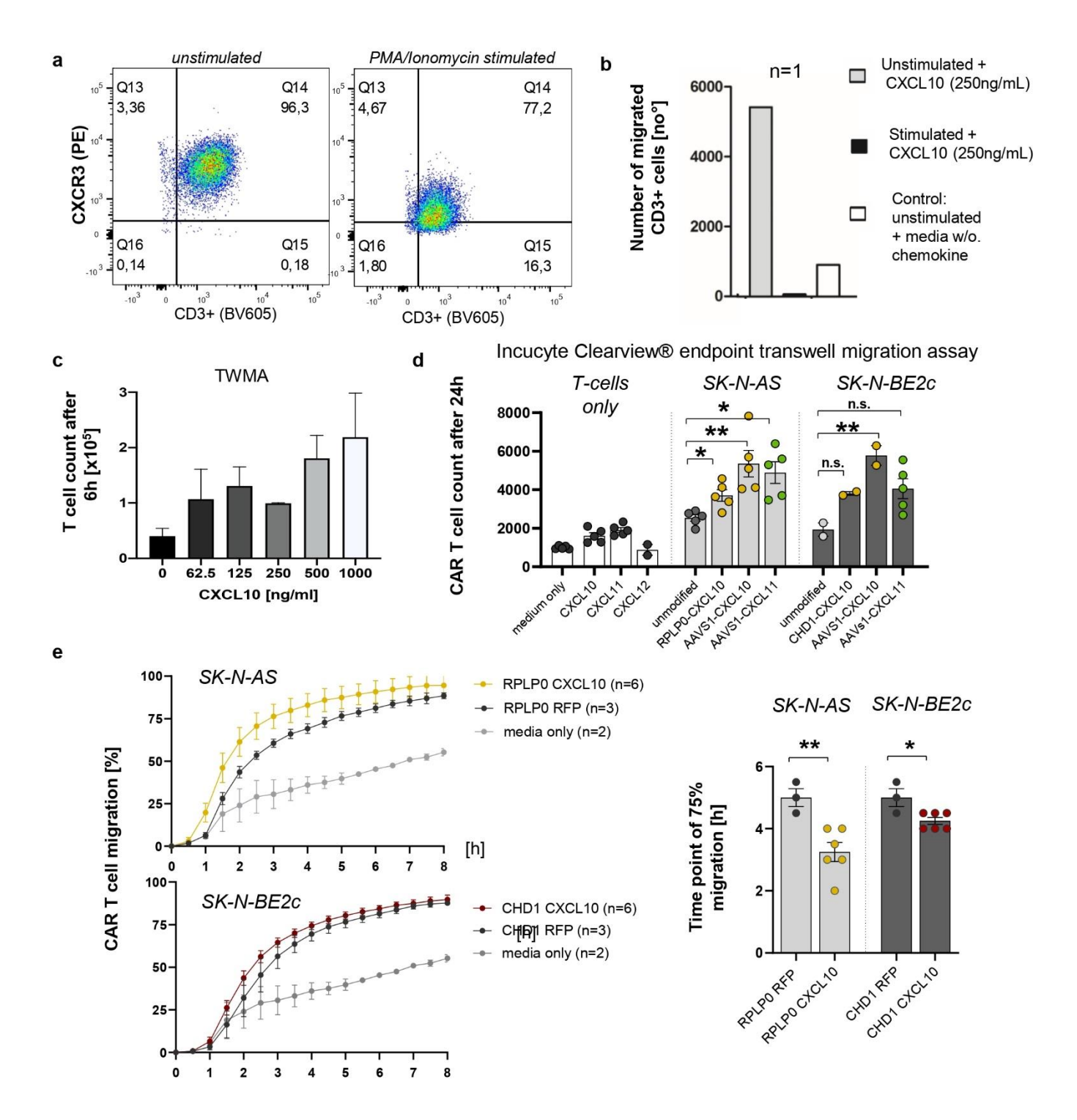
Supplementary Fig. S15. Characterization of enriched transgenic tumor cell lines. (a) Growth curves of unmodified or enriched SK-N-AS and SK-N-BE2c knock-in cell lines, represented by confluence development recorded using Incucyte live imaging, followed by growth rate comparison. (b) Viability curves of unmodified or enriched SK-N-AS and SK-N-BE2c knock-in cell lines, measured using Incucyte Cytotox Dye and Incucyte live imaging. *Data presentation:* (a,b) Means ± SD. Statistical analysis: (a) Kruskal-Wallis with Dunn's post hoc test; n.s., not significant.



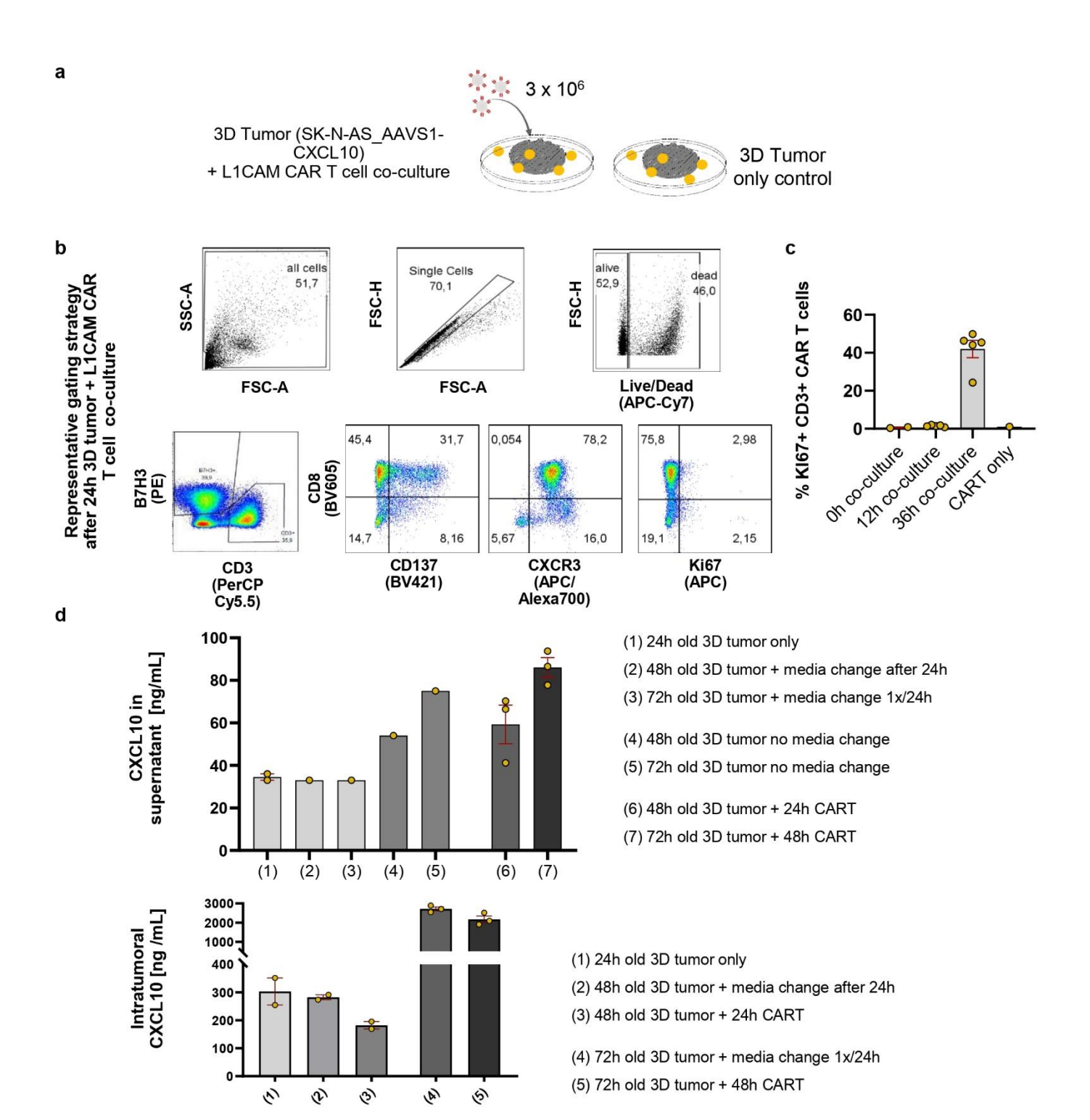
Supplementary Fig. S16. CAR T cell activation and exhaustion in tumor cell line—CAR T cell co-culture experiments. (a) Schematic overview of the two CAR constructs used in the study, featuring an EF1α promoter followed by a lentiviral 5′ long terminal repeat (LTR), a codon optimized L1CAM-targeting single-chain variable fragment (scFv), a short 12 amino acid long spacer domain from the immunoglobulin G4 (IgG4) Fc hinge, a CD28 transmembrane (tm) domain, a CD28 costimulatory (costim) domain, a CD3-zeta signaling domain, a T2A linker, firefly luciferase, a P2A linker and a truncated non-functional epidermal growth factor receptor (EGFRt). (b) T cell activation, represented by CD25 and CD137 positivity, measured via flow cytometry 24 hours after co-culture initiation (see Fig. 4) for different tumor cell line—CAR T cell combinations. (c) T cell exhaustion, represented by LAG3, TIM3 and PD1 positivity, measured via flow cytometry under the same conditions. *Data presentation: (a-c) Means ± SD. Statistical analysis: (a-c) Kruskal-Wallis with Dunn's post hoc test. p values: \*<0.05, \*\*<0.01, \*\*\*<0.001; n.s., not significant.* 



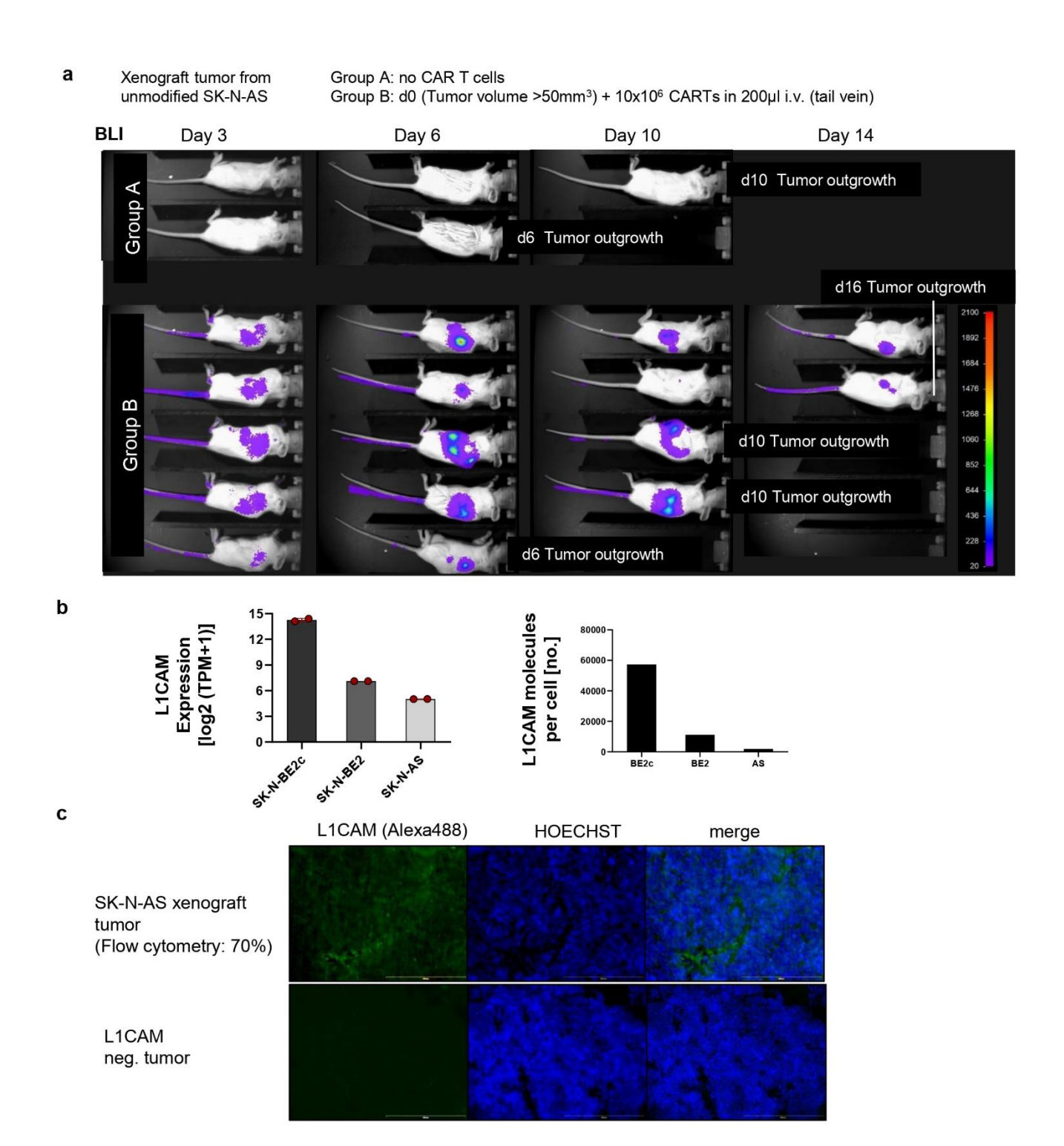
Supplementary Fig. S17. Cytokine secretion in tumor cell line—CAR T cell co-culture experiments. CXCL10, CXCL11, IFNG and IL2 cytokine concentrations in the supernatant, determined via ELISA 24 hours after co-culture initiation. Data presentation: Means ± SD. Statistical analysis: Kruskal-Wallis with Dunn's post hoc test. p values: \*<0.05, \*\*<0.01, \*\*\*<0.001; n.s., not significant.



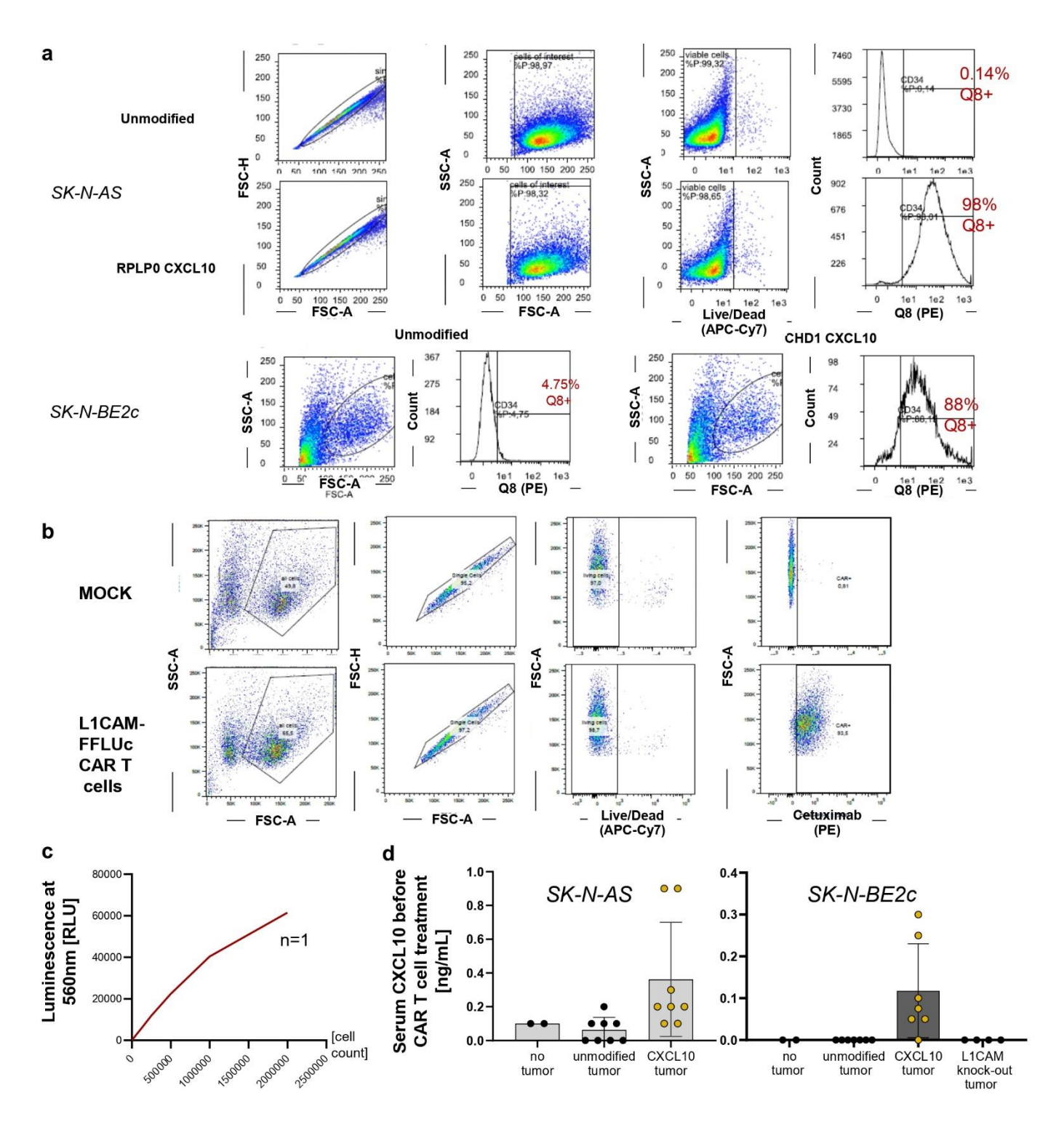
Supplementary Fig. S18. Cytokine-mediated T cell migration in vitro. (a) Representative flow cytometry data showing CXCR3 expression, the receptor for CXCL10 and CXCL11, on unstimulated and PMA (Phorbol 12-Myristate 13-Acetate)/Ionomycin-stimulated T cells. (b) Preliminary Boyden chamber transwell migration assay (Corning) comparing the number of migrated CD3<sup>+</sup> T cells between unstimulated and PMA/Ionomycin-stimulated conditions. (c) Boyden chamber transwell migration assay comparing the number of migrated CD3<sup>+</sup> T cells in response to increasing CXCL10 concentrations. (d) Incucyte Clearview endpoint transwell migration assay (Sartorius) measuring the number of migrated L1CAM-targeting CD3<sup>+</sup> CAR T cells after 24 hours in either media only, recombinant cytokines, or supernatants from unmodified or knock-in SK-N-AS and SK-N-BE2c cell lines. (e) Migration curves generated using a Boyden chamber transwell migration assay (Corning) and Incucyte live imaging (Sartorius) to determine the migration rate of CD3<sup>+</sup> CAR T cells in response to supernatants from transgenic SK-N-AS and SK-N-BE2c cell lines (CXCL10-expressing or RFP) or media only, followed by statistical comparison of the time points at which 75% of migration was reached. *Data presentation:* (c-e) Means ± SD. Statistical analysis: (d, e) Kruskal-Wallis with Dunn's post hoc test. p values: \*<0.05, \*<0.01; n.s., not significant.



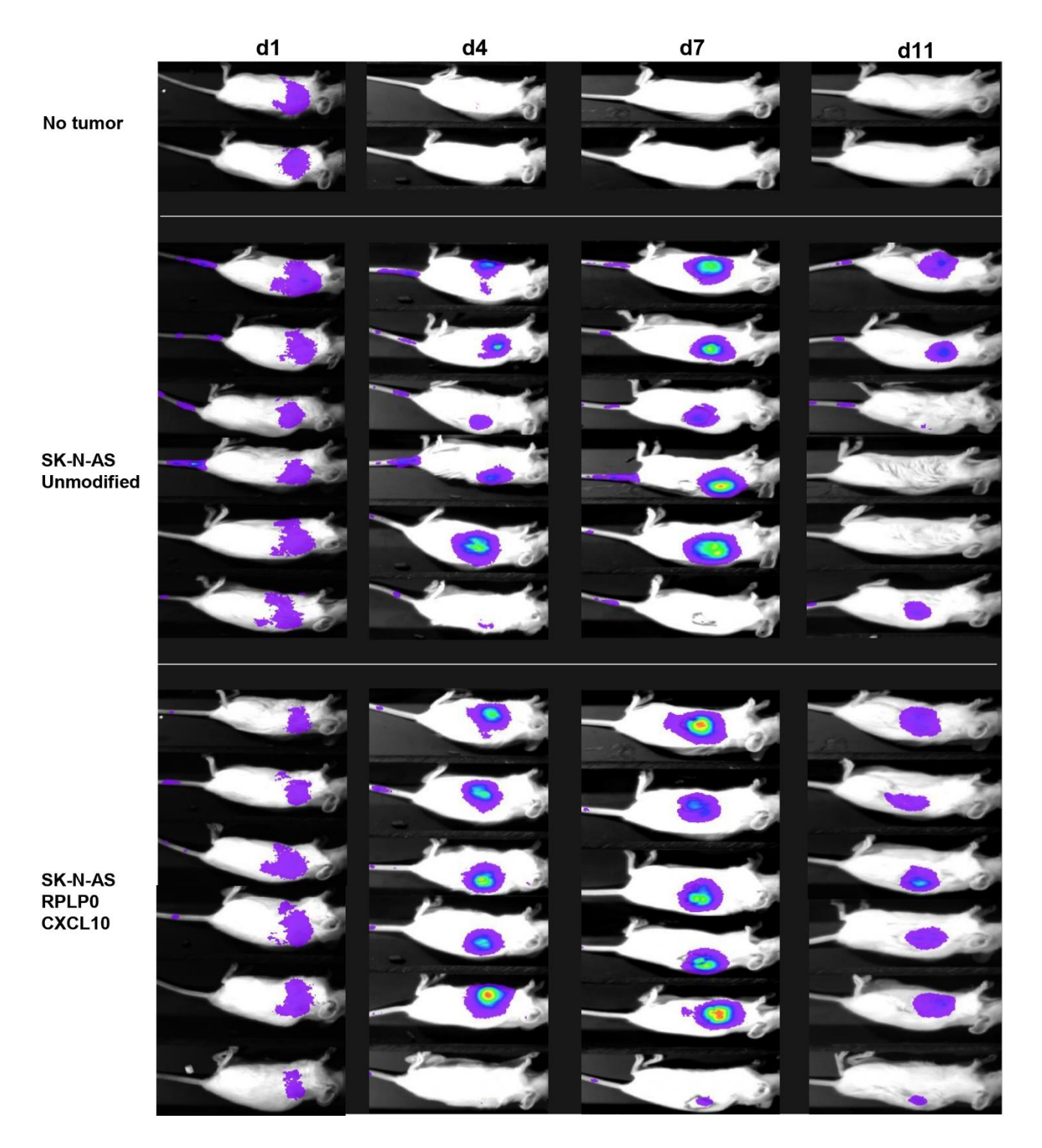
Supplementary Fig. S19. 3D tumor infiltration assay. (a) Schematic overview of the preliminary 3D bioprinted SK-N-AS tumor model and L1CAM-targeting CAR T cell co-culture. (b) Representative flow cytometry gating strategy 24 hours after 3D bioprinted SK-N-AS tumor—L1CAM CAR T cell co-culture, distinguishing T cells and tumor cells via B7H3 and CD3 surface markers. (c) K167 proliferation marker positivity in CD3<sup>+</sup> CAR T cells at different time points following 3D tumor—CAR T cell co-culture initiation. (d) CXCL10 concentration measured by ELISA in the supernatant or within the 3D tumor construct under various co-culture conditions. *Data presentation:* (c, d) *Means ± SD*.



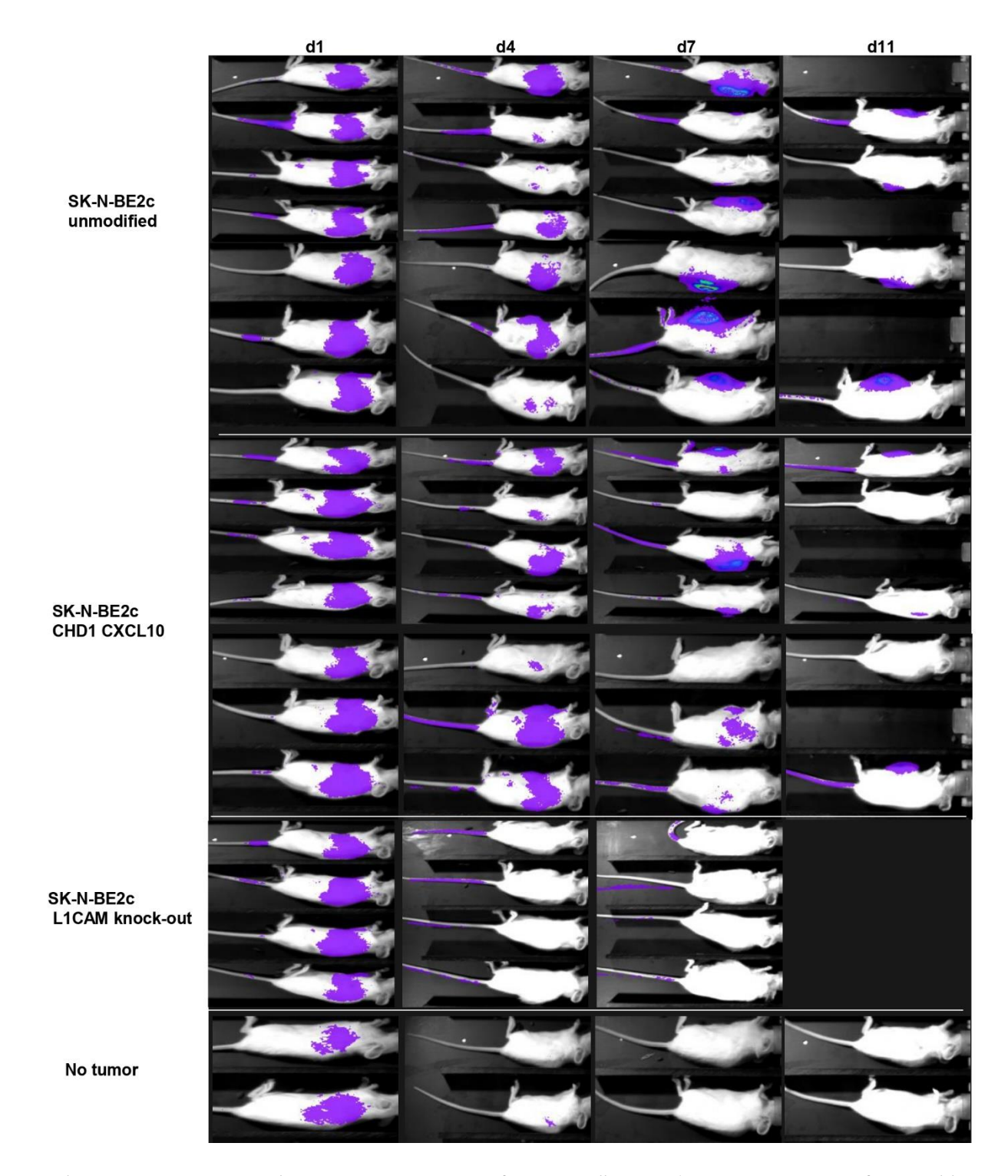
Supplementary Fig. S20. In vivo CAR T cell infiltration model development. (a) Preliminary in vivo CAR T cell infiltration analysis in a xenograft mouse model using unmodified SK-N-AS neuroblastoma cells and L1CAM-targeting, firefly luciferase-expressing CAR T cell treatment after tumor engraftment (tumor size >50 mm³), followed by regular monitoring and bioluminescence imaging to assess CAR T cell migration, tumor infiltration and expansion. (b) L1CAM expression levels from DepMap 24Q2 and 24Q4 datasets and L1CAM molecule per cell count as determined via QuantiBRITE PE bead surface expression analysis. (c) Immunofluorescence staining of two different neuroblastoma PDX mouse models, one L1CAM-positive and one L1CAM-negative. *Data presentation: (b) Means ± SD.* 



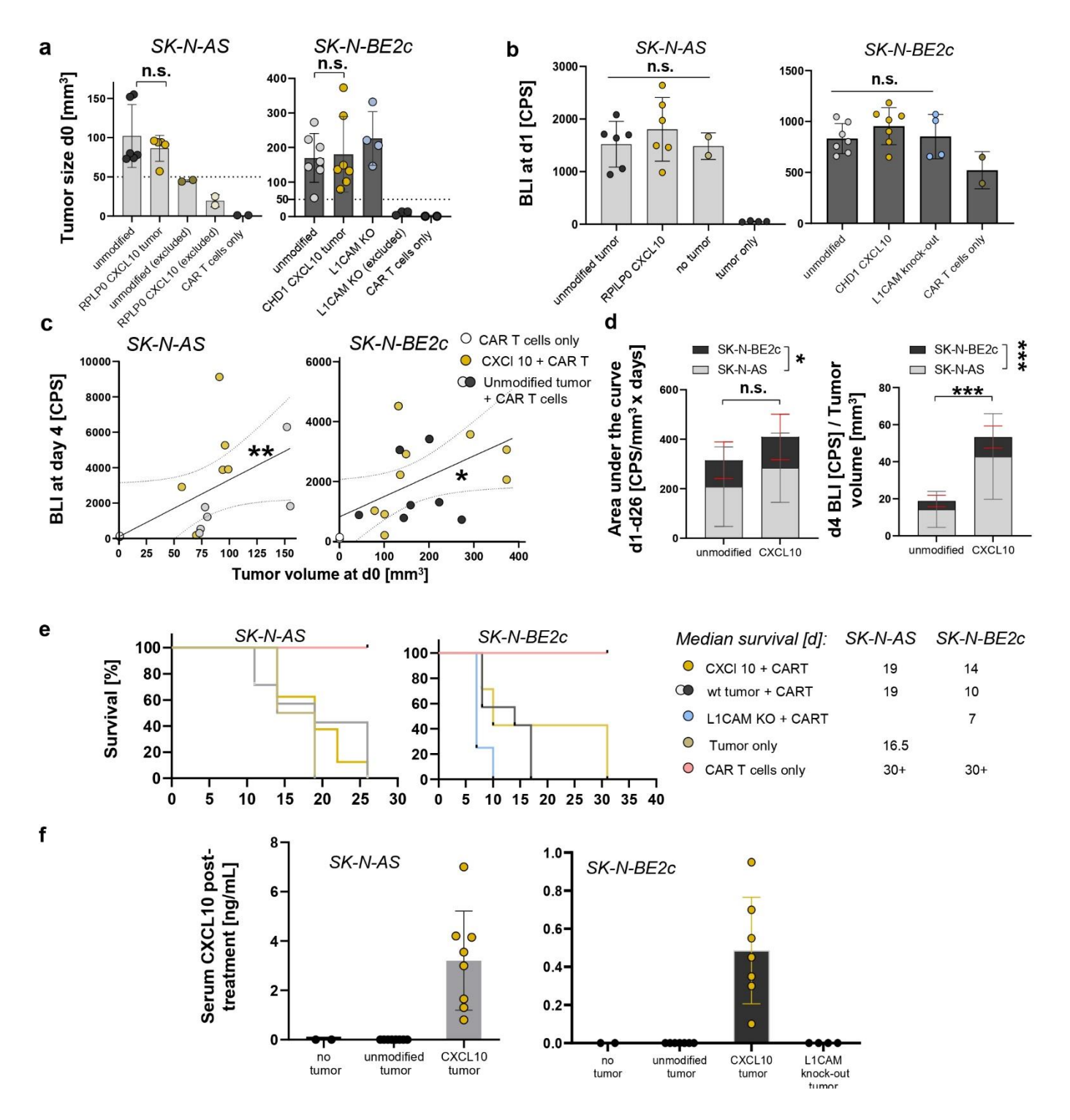
Supplementary Fig. S21. In vivo CAR T cell infiltration experiment: pre-transplant and pre-treatment analysis. (a) Confirmation of transgene expression in SK-N-AS and SK-N-BE2c neuroblastoma cell lines, assessed via Q8 positivity using flow cytometry. (b) CAR expression confirmation before in vivo application, determined by flow cytometry in CAR T cells after transduction with an L1CAM CAR, firefly luciferase and EGFRt reporter-expressing lentiviral vector, followed by expansion. Cetuximab staining was used for EGFRt detection on the cell surface. (c) In vitro bioluminescence intensity measured for different L1CAM-targeting, firefly luciferase-expressing CAR T cell counts after luciferin incubation. (d) Serum CXCL10 levels on day 0, measured by ELISA in NSG mice harboring unmodified or CXCL10-expressing SK-N-AS or SK-N-BE2c xenograft tumors, directly before CAR T cell treatment. *Data presentation: (b) Means ± SD.* 



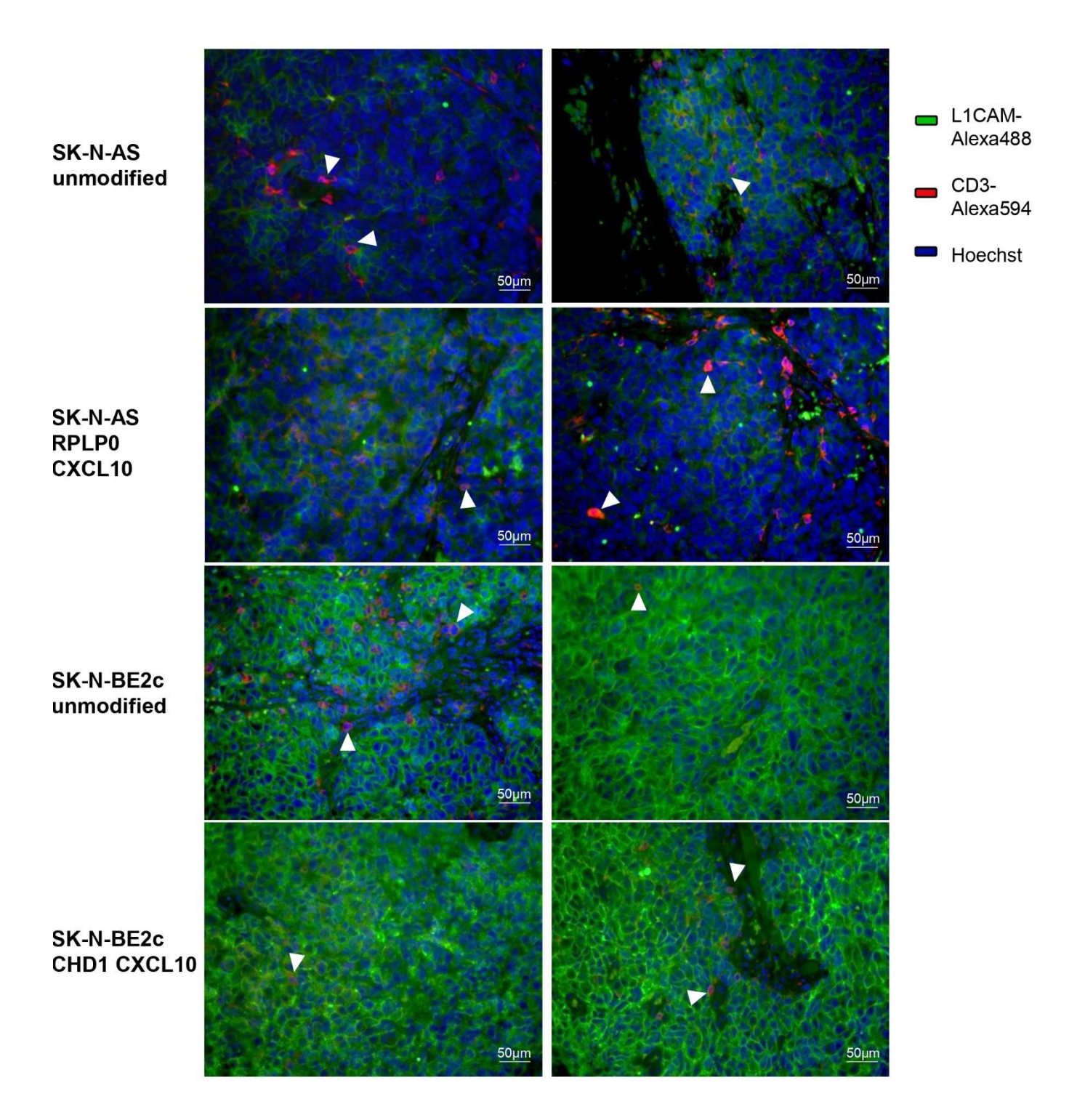
Supplementary Fig. S22. Bioluminescence imaging of CAR T cell treated SK-N-AS xenograft neuroblasoma models. Imaging timepoints are given relative to treatment with L1CAM targeting, luciferase expressing human CAR T cells. Mice with tumor volumes of >1200-1500mm³ were removed from the study. Data from d14 to d30 is not shown.



Supplementary Fig. S23. Bioluminescence imaging of CAR T cell treated SK-N-BE2c xenograft neuroblasoma models. Imaging timepoints are given relative to treatment with L1CAM targeting, luciferase expressing human CAR T cells. Mice with tumor volumes of >1200-1500mm<sup>3</sup> were removed from the study. *Data from d14 to d30 is not shown*.



Supplementary Fig. S24. In vivo CAR T cell infiltration in CXCL10-secreting xenograft tumors. (a) Manually measured tumor size on the day of CAR T cell injection (d0), compared across treatment groups; only animals with tumors bigger than 50 mm³ received CAR T cell treatment. (b) Bioluminescence measurement in the lung on day 1 after treatment with L1CAM-targeting, firefly luciferase-expressing CAR T cells. (c) Correlation between the bioluminescence signal in the left flank on day 4 and tumor volume at day 0. (d) Cumulative comparison of total tumoral CAR T cell infiltration and expansion, represented by the area under the curve (AUC) of the bioluminescence-to-tumor volume ratio and early infiltration based on the bioluminescence-to-tumor volume ratio on day 4, combining SK-N-AS and SK-N-BE2c data. (e) Survival curves for different SK-N-AS and SK-N-BE2c xenograft mouse model treatment groups after CAR T cell treatment (d0), including median survival. (f) Serum CXCL10 levels measured on the day of tumor outgrowth and animal removal after CAR T cell treatment via ELISA. Data presentation: (a, c, d, f) Means ± SD; (E) Kaplan-Meier survival curves. Statistical analysis: (a,c) Kruskal-Wallis with Dunn's post hoc test; (b) Linear regression for curve fitting and Spearman correlation. (d) Two-way ANOVA. p values: \*<0.05, \*\*<0.001; n.s., not significant.



Supplementary Fig. S25. Immunofluorescence staining of tumor sections. Representative 40x magnification images of L1CAM and CD3 immunofluorescence staining of tumor sections at the time point of outgrowth and animal removal after treatment with L1CAM-targeting, firefly luciferase-expressing CAR T cells. White arrows indicate examples of intratumoral CD3<sup>+</sup> T cells.

# **Supplementary Tables**

# Supplementary Table 1. Exemplary patient data for top and bottom rank novel PAM sites identified via CancerPAM

	Gene	Location	Variant	Expression [log 2 + 1 norm]	gRNA + PAM [5'-3']	CRISPR efficiency (Doench / Moreno Mateos)	CRISPR specificity (CFD / MIT)	rated position	copy number
Patient A								out of 110	
	QKI	Chr6:163575669	T>C	11.1	accagacaccgattgtgtgt AGG	69 / 44	94 / 89	1	2
	SARM1	Chr 17:28392620	A>G	11.9	tggactctcgaggcttgagt CGG	62 / 50	91 / 85	2	5
	PIN1	Chr19:9846446	C>G	9.1	cacaagactgtcaggcggag GGG	62 / 61	86 / 84	3	3
	EMCN	Chr4:100684664	A>C	7.6	cagctttgttctttctactt AGG	33 / 43	27 / 1	96	2
Patient B								out of 289	
	GDAP1L!	Chr20:44250939	T>C	10.5	aggcacgttgtatcaaacat CGG	64 / 62	95 / 91	1	3
	CDYL	Chr6:4844537	A>G	10.7	cacgctgctctgtccgtccg AGG	49 / 50	94 / 88	2	3
•	PTCD3	Chr2:86133390	T>C	11.8	tagccgattggccacatcca AGG	49 / 59	93 / 82	3	3
	LINC02253	Chr15:97289166	T>G	0	tattaacttgattttttaaa AGG	19 / 23	23 / 10	263	1

# Supplementary Table 2. Neuroblastoma cell line target loci

Gene	Variant	Variant RNA reads	gRNA + PAM [5'-3']	PAM Copy number	Expres- sion [TPM]	depMap CRISPR score	Doench	Moreno	CFD	MIT	CancerPAM Rank
SK-N-AS	-	•	•	•	•	-	•	•	-		out of 406
AP1M1	T>G	59%	CCGCCAGCGCCGTCTACGTG CGG	0.9	12.5	-0.06	67	67	98	96	6
SNX18	C>G	22%	GCGCTACAAGCACTTCGACT GGG	0	9.5	-0.02	52	52	99	97	8
RPLP0	A>G	62%	GCCGTGATGCCCAGGGAAGA CGG	2	16.5	-1,6	47	47	78	35	304
CHST11	T>C	50%	TTGACATCGTCCCCTTTGCG CGG	1	9.5	0	32	32	93	86	34
SK-N-BE	2c								_	·	out of 426
IGSF9B	C>G	99%	ACGGCAGCCTGACAGTGACA TGG	2.4	14	0.05	37	37	86	69	104
CHD1	A>C	33%	GAATAGTCCGTGGTCTTCCA CGG	1	12.5	0.23	44	44	94	89	36
RBM12	T>G	42%	AATAATCCATCACCCAGTGT AGG	1.2	12.5	-0.33	37	37	89	37	59
SCAF11	G>C	33%	GTAAGTGCCTCTGCCACGGT TGG	0.9	12.5	0.04	60	60	95	60	26
SH3BP1	T>C	45%	GAATTCTTGGTTGCCTGACT GGG	0	9.5	-0.06	45	45	78	45	243

## Supplementary Table 3. HDRT sequences

#### AAVS1 5'homology arm (399bp)

#### AAVS1 3'homology arm (400bp)

#### AP1M1 5'homology arm (400bp)

#### AP1M1 3'homology arm (400bp)

#### SNX18 5'homology arm (400bp)

#### SNX18 3'homology arm (395bp)

#### RPLP0 5'homology arm (400bp)

ACAGGAGCGCTATCCGCGGTTTCTGATTGGCTACTTTGTTCGCATTATAAAAGGCACGCGGGGCGCGAGGCCCTTCTCTCGCCAGGCGTCCTCGTGGAAGGTTCGTGTGCTAG
TTAGATGGGCGCCAGGGGTCGCCGGCGGGAAGCATGGAGGGCTTTTGGGGGCCTTTGGGAACATGGAGTCCTATTCTGTTCCGCCTGGGGCCTCGGTGGCGGCTTGCACGC
CCCGAGATGACGGCCGCTGCCCTAGGCAGGGCCGGCGGGGCGATTGCGCGTGTCCTCCTCTTTAGGCCCGGGACCGCGGGATGGGTGTCGGCGTGACCAGGCCTGAGCTCC
CTGTCTCTCCCTCAGTGACATCGTCTTTAAACCCTGCGTGGCAATCCCTGACGCACCGCCGTG

## RPLP0 3'homology arm (400bp)

#### CHST11 5'homology arm (400bp)

AAGCCGTAAGCGGAGGGTGCTGACCCCCAACGACCTGAAGCACTTGGTGGTGGATGAGGACCACGAGCTCATCTACTGCTACGTGCCCCAAGGTGGCCTGCACCAACTGGAAGC
GGCTCATGATGGTCCTGACCGGGCGGGGGAAGTACAGCGACCCCATGGAGATCCCGGCCAACGAGGCACACGTCTCCGCCAACCTGAAGACCCTGAACCAGTACAGCATCCCA
GAAATCAACCACCGCTTGAAAAGGCTACATGAAGTTCCTGTTTGTCCGGGAGCCCTTCGAGAGGCTAGTGTCCGCCTACCGCAACAAGTTCACCCAGAAGTACAACATCTCCTTCC
ACAAGCGGTACGGCACCAAGATCATCAAACGCCAGCGGAAGAACGCCACCCAGGAGGCC

#### CHST11 3'homology arm (400bp)

#### IGSF9b 5' homology arm (400bp)

## IGSF9b 3' homology arm (400bp)

GTCAGTCGGGAGGACAGAGGTGCCTACACCTGCCGAGCGTACAGCATTCAGGGGGAGGCTGTCCACACGACTACCTGCTTGTCCAAGGTAGGAGCCATTTCCTCAGCCTCTTT
AACCCTGGGCTCCCGCGGGGATGTCCAGCCCGGCTGAGCTACGGAGGGCGTTTTCCCAGGGCTCAGCTGGGGCTAGTGGAGGTGCAGGCGGCCATGAGGACCTGTGCGGGG
CTCCTGTGTGCTGCCTGCCTGCCCTGGTCAGAGCTCCTGCACCGGCTGCCTGGGAGAGGGCCCACAGGCCCACAGGCCGTGGCCACAGGCCCACAGGCCCACAGGCCCACAGGCCCCCCTG
CTGTGTGGGTTTCTGGTTTCTCCTTCTGTTCAGATAGCATCTCTCCCATGTCTCCGCCTCCCT

## CHD1 5'homology arm (400bp)

TTATTGATCAATGTTTCTTCACAGTTCTGATCTCCTCAGGAAAAATGCCTAGAGGTTATGTTGCTCGCGTCAGTAGAATAACTTTTGGAGGCCTTTTGATATAATGTCTGATTACCTTT
TAAATCAAAATATCCACCAGAGGTATATATTTTTCTCTGTTTGCTCTTTAATTTTGTTTATGGAATGTTTTTGATACATTTAAAACATTTTTAAAGATTCCGACCATCTTTTATAATGG
TTTTTGCTCTTAAGATACAAGCTGTTTTTACACTAAGGTTGGGTAAATATTTTCCAATTCCAGATTAGTTTCAATGGAAGTGAAGGGAGGCGCAGTAGAAGTAGGAAGTACTCTG
GATCTGATAGTGATTCCATCTCAGAAGGGAAAAGGCCCAAAGAACCGTGG

#### CHD1 3'homology arm (400bp)

## RBM12 5'homology arm (400bp)

TGTGGTTTCAGCGCAGCATGGCTGTGGTCATCCGTTTGCAAGGTCTCCCAATTGTGGCGGGGACCATGGACATTCGCCACTTCTTCTCTGGATTGACCATTCCTGATGGGGGCGTGCATATTGTAGGGGGTGAACTGGGTGAGGCTTTCATCCGTTTTTGCCACTGATGAAGATGCAAGGCTTGGTATGATGCGCACAGGTGGTACAATTAAAGGGTCAAAAGTAACACTATTGTTGAGTAGGTAAGACGGAAATGCAGAAATTGAACTGAGTCGTAGGCGTTTTGAAACTGCCAACTTAGATATACCACCAGCAAATGCCAGTAGATCAGGACCACCACCTAGCTCAGGAATGAGATGCAGCAACAGTATCCAACTTTAATAA

#### RBM12 3'homology arm (400bp)

#### SCAF11 5'homology arm (401bp)

#### SCAF11 3'homology arm (400bp)

#### SH3BP1 5'homology arm (400bp)

CCACACCAGGAGGATGCTGTGGGGTCTGCTGAGTACAGTGTGTACTTGTGCACGCCTGGTCCCTAGGAGCACAGGTGGTTAGCGTATCTGTGAGGGTGTGCCCGCGTGTGT CACAGCTGGTGCTGGGGCAACCCTAAAGCCTGGGATCCTGTAAACAGTCCTGCGGCAGCCCTGTTCTCCCCCTCTGTGGAGTGGCTGTGATCACCAAATCTGCCACCAGGGGGCA ACCCAGAGCACTCATGGCCCAGCCTGGGCAGAGGCCCCGGCCAGTGGAGCTCTCAGATCTGCAGCTCTAAATCCTAGAATCCCATGTGGTCTGCTGTATGGAGGGGACACTTG GCTCTGGACATGCAACAGGGCAGGTGACCAGCTCACCTTGGGATCATCTCCAGGCCCAGT

#### SH3BP1 3'homology arm (400bp)

#### Ef1a(s) promoter 239bp

GCTCCGGTGCCCGTCAGTGGCCAGAGCGCACATCGCCCACAGTCCCCGAGAAGTTGGGGGGAGGGTCGGCAATTGAACCGGTGCCTAGAGAAGGTGGCGCGGGGTAAACT GGGAAAGTGATGTCGTGTACTGGCTCCGCCTTTTTCCCGAGGGTGGGGGAGAACCGTATATAAGTGCAGTAGTCGCCGTGAACGTTCTTTTTCGCAACGGGTTTGCCGCCAGAA CACAGGCCGCCACC

#### CXCL10 (294bp)

#### CXCL11 (282bp)

## IFNG (498bp)

#### GFP (714bp)

## P2A (66bp)

#### Q8 reporter tag (417bp)

#### sPA (49bp)

AATAAAAGATCTTTATTTTCATTAGATCTGTGTGTTGGTTTTTTTGTGTG

HDRT: Homology Directed Repair Template, bp: base pairs

## Supplementary Table 4. Primer and probe sequences

HDRT amplification primers	Orientation	Sequence	
AAVS1_5'HA_FWD	FWD	ACCGTTTTTCTGGACAACCCC	
AAVS1_3'HA_REV	REV	AGAACTCAGGACCAACTTATTCTGATTTTGT	
AP1M1_5'HA_FWD	FWD	GTCGGTTTCACCACCAGGC	
AP1M1_3'HA_REV	REV	CTCGCCACCCCGGC	
CHD1_5'HA_FWD	FWD	TTATTGATCAATGTTTCTTCACAGTTCTGATCTCC	
CHD1_3'HA_REV	REV	TAACTTTGGGAGTCATAAACACCGTGAG	
CHST11_5'HA_FWD	FWD	AAGCCGTAAGCGGAGGGT	
CHST11_3'HA_REV	REV	GCATGATTCTCCCCTCTCCCC	
IGSF_5'HA_FWD	FWD	AAGCCCATTGTCACCTGGC	
IGSF_3'HA_REV	REV	AGGGAGGCGGAGACATGG	•
RPIPO_5'HA_FWD	FWD	AGCGCTATCCGCGGTTTCT	

RPIPO_5'HA_REV	REV	GCAGGAGAATCGCTTGAACCTG
RBM12 5'HA FWD	FWD	TGTGGTTTCAGCGCAGCATG
RBM12 3'HA REV	REV	ATTCATAGGTGCTCCAGAGCCATT
SCAF_5'HA_FWD	FWD	GGTCACCCAACAAGACACTCCAC
SCAF 3'HA REV	REV	TCATACAAATAACATATTAAATTTATAATTCTTCAAATAAAACAGTATCAATAAACCAACAAG
SH3BP1 5'HA FWD	FWD	CCACACCAGGAGGATGCTG
SH3BP1 3'HA REV	REV	CTTCATTTATTCACTCGCTCGCTC
SNX18_5'HA_FWD	FWD	CTAGATCGACGGCTCGTCTTC
SNX18 3'HA REV	REV	GTTGGCCGTGTGGTTGAGC
PAM frequency/ CRISPR cutting (out/out)	Orientation	Sequence
AAVS1_PAM freq. /Cutting_FWD	FWD	GGCATCTCTCCCTCA
AAVS1_PAM freq./Cutting_REV	REV	TGGGGACTAGAAAGGTGAAG
AP1M1_PAM freq./Cutting_FWD	FWD	TCCAAACGCCAAAACGGAGA
AP1M1 PAM freq./Cutting REV	REV	CGGCATTAGTAGGTGCTCCC
CHD1_PAM freq./Cutting_FWD	FWD	GCTCAAGTTATCTTCCTGCCTTGGC
CHD1_PAM freq./Cutting_REV	REV	GCCTGGCCAATCTTACCTCATCTC
CHST11 PAM freq./Cutting FWD	FWD	AGCCAAGTGGAAATGTTTCAGG
CHST11 PAM freq./Cutting REV	REV	AGAATGGTGGCATCCATACACA
GBA2_PAM freq./Cutting_FWD	FWD	TGCCTGGGAATATGGGGAGA
GBA2 PAM freq./Cutting REV	REV	CTAGTCCACACCCAACACCC
IGSF9b PAMfreq./Cutting FWD	FWD	CCCTGATGCTACAGGCACAA
IGSF9b PAM freq. REV	REV	CACAGGTCCTCATGGCCG
IGSF9b_Cutting_REV	REV	CTCTGCCAAATGCCCACTGT
RBM12 PAM freq. /cutting FWD	FWD	GCAAGGCTTGGTATGATGCG
RBM12 PAM freq. REV	REV	GGAGGAACTGGAATTGGGGG
RBM12_Cutting_REV	REV	GGCAGGGCTAACTTCCACAT
RPLPO_PAM freq./Cutting_FWD	FWD	AATTATGTCTCAGCTCCACGTCAT
RPLPO_PAM freq./Cutting_REV	REV	CTCAAAGGCCATCCAAAAGTCA
SCAF11 PAM freq. /Cutting FWD	FWD	GTCCACGAGGAAATGCGGT
SCAF11 PAM freq. REV	REV	AAGTCTTTCTCACGCCCAG
SCAF11_Cutting_REV	REV	TTTGGCAAGGTTTGGAGCAG
SNX18 PAM freq./Cutting FWD	FWD	GAGCTCTCATTCACCGCACT
SNX18 PAM freq./Cutting REV	REV	GATGTCCGGGAAGTTAGCCA
dPCR Primers and probes: Transgene CNV (I		G. T. G. T. G. G. G. T. T. T. G. G. T.
CXCL10_Transgene_FWD	FWD	GGAAAAGCTCGAGATCATCC
CXCL10 Transgene REV	REV	TCTTTTTCATTGTGGCGATGATT
CXCL10_Transgene_Probe	Probe	6FAM-CTGCTTCTCAGTTCTGCCCTAGAGTGG-BHQ1
CXCL11 Transgene FWD	FWD	CTACAGTTGTTCAAGGCTTC
CXCL11 Transgene REV	REV	GGTACATTATGGAGGCTTTC
CXCL11_Transgene_Probe	Probe	6FAM-ACGCTGTCTTTGCATAGGCCC-BHQ1
IFNG_Transgene_FWD	FWD	AAGGAAGAAAGCGATCGAAA
IFNG_Transgene_REV	REV	ATAGATTGGTCGTCCTTGAA
IFNG_Transgene_Probe	Probe	6FAM-TGCAATCCCAGATCGTGAGCTTCT-BHQ1
dPCR Primers and probes: Site-specific knoc		
Ef1a Out/In REV	REV	GCACTTATATACGGTTCTCC
AAVS1 Out/In FWD	FWD	GCCGTCTTCACTCGCTG
AAVS1_Out/In_Probe	Probe	6FAM-TCCCTTGCGTCCCGCCTCCCCTT-BHQ1
CHD1 Out/In FWD	FWD	GAACTCCTGGGCTCAAGTTATC
CHD1_Out/In_Probe	Probe	6FAM-ATGCTGGGATTACAGGCATGAGCT-BHQ1
RPLPO Out/In FWD	FWD	TATCCAATGGTTGCCTGTAT
RPLPO Out/In Probe	Probe	6FAM-CTATTGGCTGCCCATCGCCCGT-BHQ1
dPCR Primers and probes: Endogenous Cont		WIAMI CIAITOOCTOCOCCATCOCCCOT-DIIQI
·	FWD	CACCTAGCATGTGTGGCATT
AFF3 FWD		
AFF3 REV AFF3 probe	REV Probe	GCAGATCCAGGTCGTTGAAG  HEX-AACAACTCTTTCTGTCCCCCCT-BHQ1
LIDET Lample and Directed Bengir Templet	rione	DEVI reverse from Fraguency dDCDs digital DCD DUO1. Dlask Hale Overshor 1

HDRT: Homology Directed Repair Template, FWD: forward, REV: reverse, freq.: Frequency, dPCR: digital PCR, BHQ1: Black Hole Quencher 1.

# Supplementary Table 5. Equipment and Consumables used

Item	Catalogue n°	Provider
Equipment		
4D-Nucleofector® core unit		Lonza Bioscience
4D-Nucleofector® X Unit		Lonza Bioscience
C1000 Touch Thermal cycler		Bio-Rad
Centrifuge 5415R		Eppendorf GmbH
Centrifuge 5424		Eppendorf GmbH
Centrifuge 5427R		Eppendorf GmbH
Centrifuge 5810 R		Eppendorf GmbH
Duomax 1030, platform shaker		Heidolph instruments
Electronic Balance ABS 80-4		Kern & Sohn GmbH

Electronic Rotary Microtome HM340E		Biotek
Erlenmeyer flasks		Thermo Scientific
FlowCytometer LSR-Fortessa X-20		BD Biosciences
Fortessa Aria Cell sorter		BD Bioscience
Fortessa X-20		BD Bioscience
Freezer (-20°C) LCv4010		Carl Roth
Freezer (-80°C), HeraFreeze T series HFU400TV63		Thermo Scientific
GloMaxR Multi		Promega
Heat controlled pressure cooker		Dako
Ice machine Manitowoc SOTTO		Manitowoc
Incubator HERAcell 240i CO2		Thermo Scientific
Laminar Airflow Bench HERA safe 2020 KSP18		Thermo Scientific
Luminometer GloMaxR- Multi+Microplate Multimode		Promega
Reader with InstinctR E8032		Tromega
Magnetic Shaker RH basic		IKA Laboratoy Equipment
Manual system microscope Olympus BX43		Olympus
		Zeiss
Microscope Axio Vert.A1		
Millipore Barnstead MicroPure		Thermo Scientific
NanoDrop 2000		Thermo Scientific
Neubauer counting chamber		Brand
PCR workstation Pro		VWR Peqlab
pH-meter Five Easy Le409		Mettler Toledo
Pipette filler pipetusR		Hirschmann Labortechnik
Pipette multipipetteR stream		Eppendorf GmbH
Pipettes (2.5 – 1000 μl)		Eppendorf GmbH
QuadroMACS		Miltenyi
Qubit fluorometer		Thermo Scientific
QIAcuity Digital PCR System (6-plex)		Qiagen
Shandon Excelsior ES		Thermo Scientific
Spectrophotometer EPOCH		BioTek Instruments
StepOnePlus Real-Time PCR system		Thermo Scientific
Suction pump AC02		Carl Roth
Table centrifuge mini star silverline		VWR
ThermoMixer C		Eppendorf GmbH
Transwell Permeable supports  Ultracentrifuge Optima L90K		Costar Beckman Coulter
Vortexer Reax top		Heidolph instruments
Vortexer VWRR Galaxy Mini Star		VWR International byba
Waterbath GFL 1086		GFL Technology
General consumables		
8-Well PCR tube strips plus 8 domed caps	strips: 72.985.002, caps: 65.989.002	Sarstedt
96-Well Plate Advanced TC (flat bottom)	655983	Greiner Bio-one
Biosphere <sup>®</sup> Filter Tip 10 μl	70.1130.210	Sarstedt
Biosphere® Filter Tip 1000 μl	70.762.211	Sarstedt
Biosphere® Filter Tip 100 μl	70.760.212	Sarstedt
Cell culture multiwell plate, 6 well, PS, clear, sterile	657160	Greiner Bio-one
Cell culture plates CELLSTAR®, sterile, white-96-well plates	KL43.1	Roth
CELLSTAR®, TC, lid with condensation rings, sterile	655180	Greiner Bio-one
CryoPure Tube 1.6 ml yellow	72.380.004	Sarstedt
Disposable needles Sterican® long bevel facet, 0.30x12	4656300	B.Braun
mm		
Disposable Syringe, Luer, 1 ml	CH030001L	Charina
FACS tubes	352052	BD
Falcon® 10 ml Serological Pipet	357551	Corning
Falcon® 12-well Clear Flat Bottom TC-treated Multiwell	353043	Corning
Cell Culture Plate		

Falcon® 12-well Clear Flat Bottom TC-treated Multiwell	353043	Corning
Cell Culture Plate		
Falcon® 15 ml High Clarity PP Centrifuge Tube	352096	Corning
Falcon® 2 ml Serological Pipet	357507	Corning
Falcon® 24-well Clear Flat Bottom TC-treated Multiwell Cell Culture Plate	353047	Corning
Falcon® 24-well Clear Flat Bottom TC-treated Multiwell	353047	Corning
Cell Culture Plate	257525	
Falcon® 25 ml Serological Pipet	357525	Corning
Falcon® 35 mm TC-treated Easy-Grip Style Cell Culture Dish	353001	Corning
Falcon® 40 μm Cell Strainer	352340	Corning
Falcon® 48-well Clear Flat Bottom TC-treated Multiwell Cell Culture Plate	353078	Corning
Falcon® 5 ml Round Bottom Polystyrene Test Tube	352052	Corning
Falcon® 5 ml Round Bottom Polystyrene Test Tube, with	352235	Corning
Cell Strainer Snap Cap		Coffing
Falcon® 5 ml Serological Pipet	357543	Corning
Falcon® 50 ml High Clarity PP Centrifuge Tube	352070	Corning
FrameStar Fast Plate 96-well semi skirted	4ti-1200	4titude
Injekt Solo-2-piece single-use syringe, 10 ml, Luer Lock	201235	B.Braun
MACS LS Columns	130-042-401	Miltenyi Biotec
MACS MS Columns	130-042-201	Miltenyi Biotec
Pasteurpipette glass, 145mm	500635	Brand
Pasteurpipette glass, 230mm	500636	Brand
Reagent Reservoirs, 25 ml	EKT8.1	Carl Roth
Rotilab®-syringe filters, CA, sterile, 0.45µm	KC71.1	Carl Roth
Sodium butyrate	B5887-1g	Sigma Aldrich
Spitzen Filter Surphob 100 µl (10x96)	VT0230	
		Biozym
Spitzen Filter Surphob 10 µl lang (10x96)	VT0200	Biozym
Spitzen Filter Surphob 1,250 μl (10x96)	VT0270	Biozym Carl Roth
Stericup Sterile, Stainless Steel, Premium Disposable Scalpel,	CT92.1	
11PA	03025	Razormed
Transwell Permeable supports	10107341	Costar
Vasco® Nitril blue glove S	9205518	B.Braun
Chemicals and reagents (general)		
0.05% Trypsin-EDTA (1x)	25300-096	Gibco
2x HEPES	S0874	Takara
Albumin from bovine serum Fraktion V	8076.3	Carl Roth
Anti-human CD28 antibody	302934	Biolegend
Anti-PE microbeads	130-105-639	Inv <b>l</b> Yliberyi
Brefeldin A	#347688	BD Biosciences
CD3 antibody anti-human, pure-functional grade clone	130-093-387	Miltenyi
OKT3	130-033-307	Willerigh
CD8 microbeads, human - lyophilized	130-097-057	Miltenyi
CS&T Research Beads	655050	Becton Dickinson
Cut Smart Buffer	NEB#B6004	
		New England Biolabs  Perkin Elmer Inc.
D-Luciferin  Dimothyl sulfovida (DMSO)	122799	
Dimethyl sulfoxide (DMSO)	A994.1	Carl Roth
DISPASE II	D4693-1G	Sigma Aldrich
Dnase I	A3778.0100	AppliChem
Dynabeads Human T-Activator CD3/CD28	11131D	ThermoFisher
Dynabeads Mouse T-Activator CD3/CD28	114530	ThermoFisher
Ethanol Rotipuran 99.8% p.a.	2065.2	Carl Roth
Fetal Bovine Serum (FBS) SUPERIOR	S0615-500ML	Merck
Ficoll Paque Plus	17144002	Cytiva
Flow-Set Pro Fluorospheres	A62492	Beckman Coulter

FlowCheck Beads	A63493	Beckman Coulter
FlowClean Cleaning Agent	A64669	Beckman Coulter
Glycine Buffer ≥ 99% p.a.	3908.3	Carl Roth
H <sub>2</sub> O <sub>2</sub> (2N)	339741	Sigma Aldrich
Human IL-15, premium grade	130-095-765	Miltenyi
Human IL-7, premium grade	130-095-362	Miltenyi
Human Fc Receptor Blocking Solution	422301	Biolegend
Hydrocortisone	H0396-100MG	Sigma Aldrich
Ionomycin	10364-1MG	Sigma Aldrich
IsoFlow Sheath Fluid	8546859	Beckman Coulter
Isoflurane (CPS)	1214	Cp-pharma
KAPA HiFi HotStart Ready Mix	7958927001	Roche
L-Glutamine	25020-081	Life Technologies
LE Agarose	240004	Biozym
Live/Dead Fixable Near IR (780) Viability Kit, for 633 nm	L34975	ThermoFisher Scientific
excitation	L34973	mermorisher scientific
Matrigel	356237	Corning
Monensin	M5273-500MG	Sigma Aldrich
Nuclease-free water	1097705	Invitrogen
Papain from papaya latex buffered aqueous solution	P3128-100MG	Sigma Aldrich
Penicillin-Streptomycin (10,000 U/mL)	18140122	Gibco
PhosSTOP	4906837001	Sigma Aldrich
PMA	P8139-1MG	Sigma Aldrich
Potassium chloride (KCl) ≥ 99.5% p.a.	6781.1	Carl Roth
Potassium dihydrogen phosphate (KH <sub>2</sub> PO <sub>4</sub> ) ≥ 99% p.a.	3904.1	Carl Roth
Potassium hydrogen carbonate (KHCO₃) ≥ 99%	X887.1	Carl Roth
Powdered milk, blotting grade	T145.3	Carl Roth
Precision Plus Protein Standards	161-0374	Bio-Rad
Q5 Polymerase	M0491L	New England Biolabs
Retronectin	T1008	Takara
SDS Pellets ≥ 99.9%	CN30.3	Carl Roth
TEMED ≥ 98.5%	2367.1	Carl Roth
Tris Bufferan® ≥ 99.9% p.a.	4855.5	Carl Roth
Trypan Blue Solution 0.4%	15250061	Gibco
Tween®20	9127.2	Carl Roth
Vibrant™ Dio Cell-Labeling Solution	V22886	ThermoFisher
β-Mercaptoethanol 99% p.a.	4227	Carl Roth
Cell culture media		
RPMI Medium 1640 (1x)	21875-034	Life Technologies
DMEM (1x) Dulbecco's Modified Eagle Medium	41966052	Life Technologies
Endothelial Cell Growth Medium 2	C-22111/39211	PromoCell
Opti-MEM	31985062	Life Technologies
MCDB 131 Medium	10372019	ThermoFisher
Freezing medium	10% DMSO, 90% fetal calf serum (FCS)	
Tumor cell and HEK 293T cell medium with RPMI	RPMI Medium 1640 (1x), 10% FCS	
Tumor cell medium with DMEM	DMEM (1x), 10% FCS	
T cell (human) medium	RPMI Medium 1640 (1x), 10%	
- cen (naman) mediam	FCS, 2 mM L-Glutamin	
HDRT-generation	MOAOAS	NED
Q5 Hot Start High-Fidelity 2X Master Mix	M0494S E2621L	NEB NEB
NEBuilder HiFi DNA Assembly Master Mix	200315	Agilent
XL10-Gold Ultracompetent Cells		
Kapa HiFi Hot Start ready mix	KK2602/7958935001	Roche
AMPure XP, 60 mL	A63881	Beckman Coulter

DynaMag2	12321D	Thermo Fisher Scientific
Dpnl	R0176S	New England Biolabs
Effectene Transfection Reagent	301425	Qiagen
CRISPR knock-in		
Alt-R® S.p. Cas9 Nuclease V3, 500 μg	1081059	IDT
Poly-L-glutaminsäure Natriumsalz	P4761-100MG	Sigma-Aldrich
SF Cell Line 4D-NucleofectorTM X Kit L	V4XC-2024	Lonza
P3 Primary Cell 4D-NucleofectorTM X Kit L	V4XP-3024	Lonza
dPCR		
Pipet-Lite Multi Pipette L8-200XLS+	17013805	Mettler-Toledo
Rainin Pipette Tips TR LTS 200 μL F 960A/10	17014963	Mettler-Toledo
Eppendorf twin.tec® PCR Plate 96, semi-skirted, clean	30128575	Eppendorf
DNA LoBind® Tubes	30108051	Eppendorf
QIAamp DNA Mini Kit (50)	51304	Qiagen
QIAcuity Probe PCR Kit (5 ml)	250102	Qiagen
QIAcuity Nanoplate 26k 24-well (10)	250001	Qiagen
QIAcuity Nanoplate 26k 8-well (10)	250031	Qiagen
QIAcuity Nanoplate 8.5k 24-well (10)	250011	Qiagen
QIAcuity Nanoplate 8.5k 96-well (10)	250021	Qiagen
Nanoplate Seals (11)	250099	Qiagen
Nanoplate Tray	250098	Qiagen
Xbal	R0145S	New England Biolabs
Incucyte		
Incucyte® Clearview 96-well Reservoir Plate	4600	Sartorius
Incucyte® Clearview 96-well Plate for Chemotaxis	4582	Sartorius
Recombinant Protein G	101200	Invitrogen (Thermo)
ICAM-1 Protein, Human, Recombinant (ECD, His & hFc	10346-H03H	SinoBiological
Tag)		
Incucyte® Cytotox Dye for Counting Dead Cells: Green	4633	Sartorius
Incucyte® Nuclight Rapid Red Dye for Live-Cell Nuclear	4717	Sartorius
Labeling		
CAR T cells and Cytokine effects		
CD8 <sup>+</sup> T cell isolation kit, human	130-096-495	Miltenyi
Pan T cell isolation kit, human	130-096-536	Miltenyi
Human CXCL10/IP-10 DuoSet ELISA, 15 Plate	DY266	R&D
Recombinant human CXCL10	300-12-35	Peprotec
Human CXCL11/I-TAC DuoSet ELISA	DY672	R&D
Recombinant Human I-TAC (CXCL11)	300-46	Peprotec
Human IFN-gamma Recombinant Protein, PeproTech®	300-02-100UG	Thermo fisher
Human IFN-gamma ELISA Kit	DIF50C	R&D
Human IL-2 ELISA	555190	Becton Dickinson
pCMV-Rev2 (p13.33)		Takara
Viral Packaging PCHGP-2 (p14.36)		Takara
pCMV-G (p15)		Takara
UltraPure™ BSA (50 mg/mL)	AM2616	Thermo Fisher Scientific
ICAM-1	#10346-H03H	Sino Biological
Protein G	#101200	Thermo Fisher
96-well Essen ClearView Reservoir,	4600, 4601	Sartorius
Effectene	301425	Qiagen
Optimem I	31985070	Gibco

# Supplementary Table 6. Antibodies used for flow cytometry and IF Staining

Antibodies	Clone	Dilution	Catalogue no.	Provider
Invitrogen, CD34 Monoclonal	537860	1:10	#MA1-10205	ThermoFisher
Antibody (QBEND/10), PE				Scientific

CXCR3 (CD138) Alexa Fluro 700			353741	Biolegend
human Ab, Clone G025H7, Mou	se			
lgG1				
CXCR3, PE		1:25	353706	Biolegend
CXCR3, AX700		1:25	353741	Biolegend
B7H3, APC				Biolegend
B7H3, PE			331606	Biolegend
L1CAM (CD171), APC	REA163	1:100	130-124-024	Miltenyi
L1CAM (CD171), PE	REA163	1:100		Miltenyi
CD4, FITC		1:400	357406	Biolegend
CD4, BV421	RPA-T4	1:50		Biolegend
CD8, PerCP		1:400		Biolegend
CD8, BV605	SK1	1:400		
CD3, Ax700	HIT3a	1:400	300324	Biolegend
CD3, FITC	HIT3a	1:400		Biolegend
CD3, PerCP-Cy5.5	HIT3a	1:400		Biolegend
CD137, BV421	4B4-1	1:50	309819	Biolegend
CD137, BV605	4B4-1	1:50		Biolegend
CD25, PE-Cy7	BC96	1:100	302611	Biolegend
CD25, Ax700	BC96	1:25		Biolegend
EGFRt (Cetuximab), PE		1:100	537860	Invitrogen

# Supplementary Table 7. Software used

Software	Use	Provider
FlowJo_v.10.6.2	Analysis of flow cytometry data	FlowJo
Gen5_v2.04	ELISA assay measurement	BioTek
GraphPad PRISM_v8 to v10	Data analysis and graphical presentation	GraphPad
Incucyte 2021B	Analysis of live cell imaging	Essen Bioscience
		Free software, Copyright (c) 2006,
Primer3Plus	Primer design and adjustment	2007 by Andreas Untergasser and
		Harm Nijveen
ProSort_v1.6	FACS Sorter	Bio-Rad
SAP	Patient data collection	SAP SE
SnapGene	Development of cloning strategies, new Plasmids	Dotmatics
StepOne Software_v2.3	qRT-PCR set-up and analysis	Applied Biosystems
VisionCapt_v16.16d	Western Blot visualization	Fusion
Python version 3.11.4.	CancerPAM programming	
Visual Studio Code (Version: 1.80.1)	source-code editor	
Snakemake	Pipeline workflow management system	